Short Title

Title

By

Ian D. Roberts, B.Sc.

A Thesis

Submitted to the School of Graduate Studies

in Partial Fulfilment of the Requirements

for the Degree

Master of Science

McMaster University

Master of Science (2016) McMaster University

(Physics and Astronomy) Hamilton, Ontario

TITLE: Title

AUTHOR: Ian Roberts, B.Sc. (McMaster University)

SUPERVISORS: Laura Parker

NUMBER OF PAGES: xiii, 72

Abstract

Abstract...

Acknowledgements

Acknowledgements here

dedication here

Table of Contents

List of Figures

List of Tables

Chapter 1

Introduction

1.1 Galaxy properties

1.1.1 Color

Color is one of the simplest measures with which one can characterize the properties of a galaxy. The color of a galaxy is defined as the difference between the magnitudes of a galaxy in two different bands. As an example, the $g-r$ colour for a SDSS galaxy would be the difference between the galaxy's g-band magnitude (centred on 477.0 nm) and r-band magnitude (centred on 623.1 nm). Many studies have shown the colour distributions of galaxy populations to be well fit by a double-Gaussian across many environments **(REFERENCE)**. The two components of the double-Gaussian fit are referred to as the 'red sequence' and the 'blue cloud'. In Fig. 1.1 I show the $g-r$ colour distribution for a sample of low-redshift ($z < 0.05$) SDSS group galaxies, and a double-Gaussian fit (black) as well as the two components corresponding to the blue cloud and the red sequence. The red sequence peaks at red colours and has

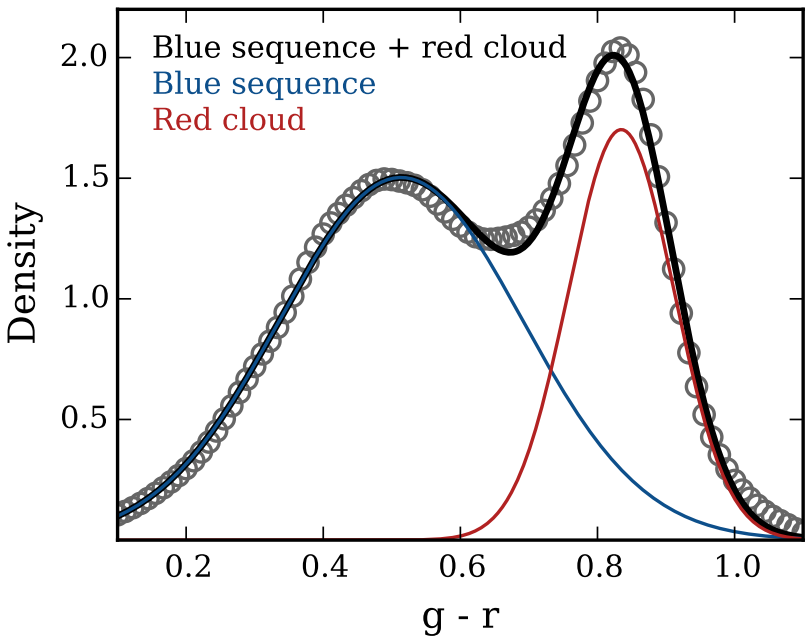

Figure 1.1 $g - r$ colour distributions for low-redshift galaxies in SDSS groups. Circles correspond to the smoothed density distribution of the data, the black line shows a double-Gaussian fit, and the red and blue lines show the components of the double-Gaussian fit corresponding to the red sequence and the blue cloud.

a relatively small dispersion, whereas the blue cloud is a bluer and broader sub-population.

The overlap region between the red sequence and the blue cloud is known as the "green valley" and is thought to be a transition region. It has been hypothesized that galaxies evolve from the blue cloud, through the green valley, onto the red sequence over time **(REFERENCE)**. An important piece of evidence in support of this evolutionary scenario is the Butcher-Oemler (BO) effect. The BO effect is an observed positive correlation between the fraction of blue galaxies within galaxy clusters and redshift, first observed by Butcher & Oemler (1978) and subsequently observed by many more recent studies (e.g.

Butcher & Oemler, 1984; Ellingson et al., 2001; Loh et al., 2008; Urquhart et al., 2010). Therefore it seems that at early times populations of galaxies in clusters were bluer than they are at present day.

1.1.2 Morphology

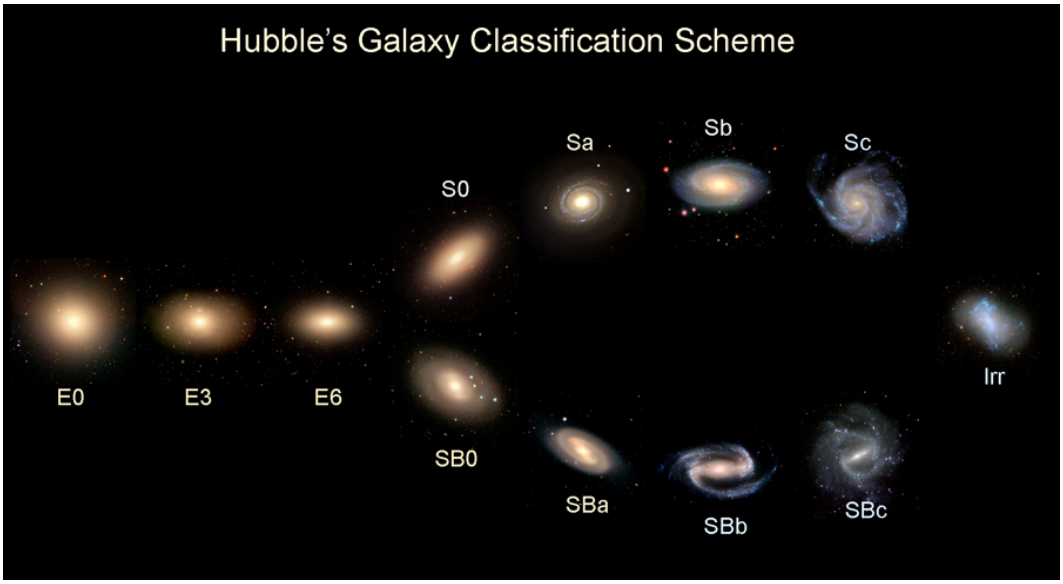

Figure 1.2 The Hubble tuning fork classification diagram. Image credit: Galaxy Zoo.

The first robust classification scheme for galaxies was laid out by Hubble (1926). This classification scheme (see Fig. 1.2), which has since become known colloquially as Hubble's tuning fork diagram, broadly divides the galaxy population into elliptical and spiral galaxies. The class of ellipticals is further sub-divided by ellipticity, $e = 0, 1, 2, ..., 7$, where $e = 10 \times (a - b)/a$, with a and b denoting the major and minor axis of the ellipse, respectively. Ellipticals can then be classified as Ee, where E0 would be perfectly round (in projection) and E7 would be a highly elongated ellipse. Spiral galaxies are

sub-classified by the brightness of the central region as well as how tightly coiled are their spiral arms. Spirals denoted as Sa are galaxies with bright central bulges and tightly wound spiral arms, galaxies denoted as Sc are galaxies with weak bulges and loosely wound spiral arms, and Sb spirals represent an intermediate class between the two. Spirals are also divided by the presence of a bar, or lackthereof, with barred spirals being denoted as SB galaxies. S0 or lenticular galaxies appear to have structure intermediate between ellipticals and spirals are characterized by a strong bulge region, as well as the presence of a disc devoid of spiral arms. Following the nomenclature used by Hubble, it is commonplace to refer to elliptical and S0 galaxies as "early-types" and spiral galaxies as "late-types", due to their positions on the tuning fork diagram. It is however important to note that this nomenclature refers solely to the position on the diagram and is agnostic to evolutionary theories[1].

Modern techniques often rely on photometric measurements of light profiles of a galaxies to classify morphology. In particular, two main measures known as the single Sérsic index (n), and the bulge-to-total ratio (B/T) are commonly used to quantitatively determine the morphology of a galaxy.

The Sérsic index, n, is a free parameter of the so-called Sérsic profile (Sersic, 1968) which often fit to galaxy intensity profiles. Using the Sérsic profile, the intensity of a galaxy as a function of radius is given by

[1] Though not always given credit, Hubble was very clear on this point stating that the classification was made "without prejudice to theories of evolution", and that "temporal connotations are made at one's peril"

$$I(r) = I_e \exp\{-k[(r/r_e)^{1/n} - 1]\}, \tag{1.1}$$

where r_e is the effective radius which encloses half of the total light, I_e is the intensity at the effective radius, and k is a normalization factor which depends on the Sérsic index n. In general, the Sérsic index runs between $1 \leq n \leq 8$. Disc dominated, spiral galaxies have light profiles which are well fit by a Sérsic index of $n \lesssim 2$, with the special case of a purely exponential disc being given by $n = 1$. Elliptical galaxies have more centrally concentrated light profiles, and are therefore well fit by larger Sérsic indices, $n \gtrsim 2$. A commonly used empirical law to describe the brightness profiles of elliptical galaxies is de Vaucouleurs' law which states that the intensity of an elliptical galaxies goes as $\log I(r) \propto r^{1/4}$, and this is also just a special case of the Sérsic profile with $n = 4$.

Instead of modelling the light profile a galaxies as a single component, bulge + disc decompositions are often used as another method of classifying the morphology of galaxies. In this scenario the light profile of the bulge and disc are modelled separately, it is common to model the bulge with an $n = 4$ de Vaucouleurs profile and the disc with an $n = 1$ exponential profile (e.g. Simard et al., 2002), the sum of these two components is then the model for the galaxy as a whole. The fraction of the total light produced in the bulge component is the bulge-to-total ratio (B/T) which is used as a morphological discriminator for galaxies. Pure elliptical galaxies will have $B/T \to 1$, and pure disc galaxies will have $B/T \to 0$.

1.1.3 Star formation rates

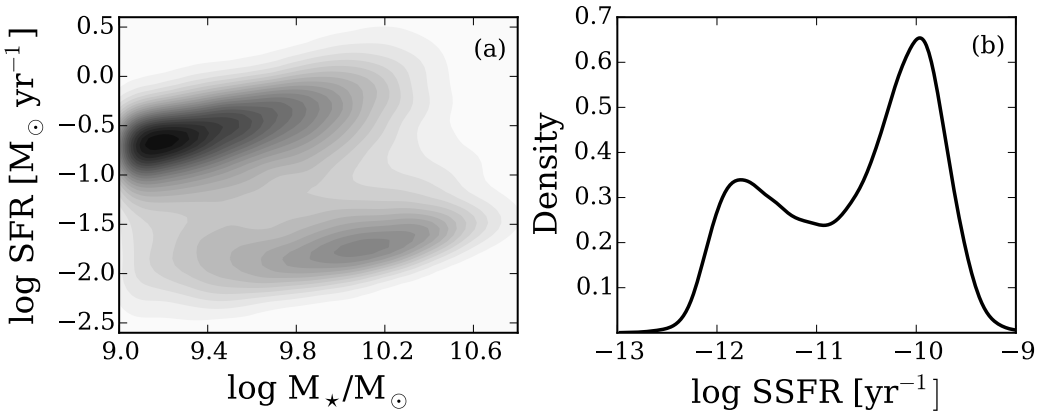

Figure 1.3 Left: Star formation rate versus stellar mass for a sample of low-redshift SDSS group galaxies. Right: Specific star formation rate density distribution for a sample of low-redshift SDSS group galaxies.

The star formation rate (SFR) of a galaxy is defined intuitively as the rate at which a galaxy generates new mass in the form of stars, measured in units of solar-masses per year ($M_\odot\,yr^{-1}$). Being able to accurately determine the SFRs of galaxies is crucial for the study of galaxy evolution. Currently there are multiple methods used to derive SFRs for galaxies, each relying on different aspects of galactic electromagnetic emission.

One of the most common methods is to derive SFRs from UV or IR continuum emission using conversion factors. UV continuum emission directly probes light emitted from young stars and therefore is a strong indicator of a galaxies SFR. The largest shortcoming of UV emission is the fact that the existance of large amounts of interstellar dust causes galaxies to be relatively opaque to UV photons. In fact, approximately half the emission from stars in the Universe is absorbed and re-emitted by dust in the infrared (Kennicutt & Evans, 2012).

The leads to IR continuum emission from dust being a useful probe of galaxy SFRs. As mentioned previously, both UV and IR continuum luminosities can be converted to SFRs using wavelength-dependent conversion factors.

In addition to continuum emission, emission line strengths can also be used as star formation indicators, with the Hα line being the most commonly used emission line indicator for galaxies in the local Universe. As before, using the correct conversion factor one can determine a SFR estimate from Hα emission, and similar to the UV continuum, the largest decrement to this method is dust attenuation. Kennicutt & Evans (2012) provide a compilation of up to date SFR conversion factors for both continuum and line emission, across a wide range in wavelength.

Another common star formation indicator is the 4000 angstrom break (D_n4000), which refers to the strength of the break at 4000 Å in a galaxy's spectrum. Galaxies with old stellar populations and little recent star formation will show a strong D_n4000 break due to strong metal absorbtion in the atmospheres of old stars as well as a lack of UV emission from young, hot stars **(REFERENCE)**. Galaxies with strong recent star formation will show a correspondingly small break at 4000 Å.

SED fitting...

Across a wide range of environments galaxies can be divided into two main subpopulations based on their SFRs, those galaxies which are actively forming stars and those quiescent galaxies whose star formation has ceased **(REFERENCE)**. One way to define the population of star-forming galaxies is to use the "star-forming main sequence" (SFMS). The SFMS is a tight correlation be-

tween SFR and stellar mass located in the upper region of SFR$-M_\star$ plane. The SFMS for low-redshift galaxies in SDSS groups is easily visible in Fig. 1.3(a) ranging between $\sim -1 < \log \mathrm{SFR} < 0$. Due to the correlation between SFR and stellar mass, it is useful to normalize SFR by galaxy stellar mass, known as the specific star formation rate (SSFR = SFR/$M_\star$). Like the distribution of galaxy color, the SSFR distribution for galaxy populations is also bimodal (see Fig. 1.3(b)). This bimodality in SSFR provides another method for distinguishing between star-forming and passive galaxies. Recent observations have shown that across many environments in the local Universe, the division between the active and quiescent populations (ie. the local minimum in the SSFR distribution) is found at $\log \mathrm{SSFR} \simeq -11$ (**?**).

1.2 The environmental dependence of galaxy properties

1.2.1 Local density

One of the first examples of the dependence of galaxy properties on environment is the observation that the fraction of early-type galaxies increases with local galaxy number density(Dressler, 1980), now known as the Morphology-Density relationship.

Bibliography

Butcher, H. & Oemler, Jr., A. 1978, ApJ, 219, 18

—. 1984, ApJ, 285, 426

Dressler, A. 1980, ApJ, 236, 351

Ellingson, E., Lin, H., Yee, H. K. C., & Carlberg, R. G. 2001, ApJ, 547, 609

Hubble, E. P. 1926, ApJ, 64

Kennicutt, R. C. & Evans, N. J. 2012, ARA&A, 50, 531

Loh, Y.-S., Ellingson, E., Yee, H. K. C., Gilbank, D. G., Gladders, M. D., & Barrientos, L. F. 2008, ApJ, 680, 214

Sersic, J. L. 1968, Atlas de galaxias australes (Observatorio Astronomico, Universidad Nacional de Cordoba)

Simard, L., Willmer, C. N. A., Vogt, N. P., Sarajedini, V. L., Phillips, A. C., Weiner, B. J., Koo, D. C., Im, M., Illingworth, G. D., & Faber, S. M. 2002, ApJS, 142, 1

Urquhart, S. A., Willis, J. P., Hoekstra, H., & Pierre, M. 2010, MNRAS, 406, 368

Chapter 2

Mass segregation trends in SDSS galaxy groups

2.1 Introduction

It has been well established that galaxy properties dpend strongly on local environment (e.g. Oemler, 1974; Hogg et al., 2004; Blanton et al., 2005a; Tal et al., 2014). Galaxies in dense environments such as clusters tend to have lower star formation rates (SFRs), while isolated field galaxies are generally actively forming stars (e.g. Balogh et al., 2000; Ball et al., 2008; Wetzel et al., 2012). It is also well known that galaxy properties, such as SFR, depend strongly on galaxy mass (e.g. Poggianti et al., 2008). It is critical to study the distribution of galaxy masses within haloes of different masses in order to ascertain whether the variations in galaxy properties with environment are due to physical mechanisms acting in dense environments, or simply due to the fact that high-density environments contain more high-mass galaxies. Intermediate-density environments, galaxy groups, represent not only the most common environment in the local Universe (Geller & Huchra, 1983; Eke

et al., 2005), but also represent the environment where many physical processes are efficient. Galaxy interactions such as mergers and harassment are favoured in this environment because of the low relative velocities between galaxies (Zabludoff & Mulchaey, 1998; Brough et al., 2006).

The study of mass segregation in groups can be used to elucidate information on physical processes such as dynamical friction, galaxy mergers, and tidal stripping. Mass segregation in bound structures has generally been predicted as a result of dynamical friction (Chandrasekhar, 1943). Dynamical friction acts as a drag force on orbiting bodies and massive galaxies within groups and clusters are expected to migrate to smaller radii as time progresses. If dynamical friction is a dominant factor, then clear mass segregation should be observed in evolved groups and clusters.

Galaxy groups are not static systems, but are constantly being replenished by infalling galaxies from the field. Infalling galaxies are preferentially found at large radii (Wetzel et al., 2013) and the difference in stellar mass distributions between evolved group members and infalling galaxies could affect the strength of mass segregation.

If significant mass segregation is not found, then this implies that either: the time-scale associated with dynamical friction is greater than the age of the group/cluster, or that there are other physical processes, such as merging, tidal stripping, or pre-processing, which are playing a more important role than dynamical friction.

Recent work has shown conflicting results with regards to the presence of mass segregation in groups and clusters. Ziparo et al. (2013) find no evidence

for strong mass segregation in X-ray selected groups out to $z = 1.6$, for a sample of galaxies with $M_{\rm star} > 10^{10.3}{\rm M}_{\odot}$. von der Linden et al. (2010) examine Sloan Digital Sky Survey (SDSS) galaxy clusters and find no evidence for mass segregation in four different redshift bins at $z < 0.1$. von der Linden et al. make redshift-dependent stellar mass cuts ranging from $10^{9.6}$ to $10^{10.5}{\rm M}_{\odot}$. Vulcani et al. (2013) use mass-limited samples at $0.3 \leq z \leq 0.8$ from the IMACS Cluster Building Survey and the ESO Distant Cluster Survey, with stellar mass cuts at $M_{\rm star} > 10^{10.5}{\rm M}_{\odot}$ and $M_{\rm star} > 10^{10.2}{\rm M}_{\odot}$, respectively, to study galaxy stellar mass functions in different environments. Vulcani et al. find no statistical differences between mass functions of galaxies located at different cluster-centric distances.

Conversely, Balogh et al. (2014) find evidence for mass segregation in Group Environment Evolution Collaboration 2 (GEEC2) groups at $0.8 < z < 1$, using as stellar-mass-limited sample with $M_{\rm star} > 10^{10.3}{\rm M}_{\odot}$. Using a volume limited sample of zCOSMOS groups, Presotto et al. (2012) find evidence for mass segregation in their whole sample at both $0.2 \leq z \leq 0.45$ and $0.45 \leq z \leq 0.8$. Presotto et al. also break their sample into rich and poor groups at $0.2 \leq z \leq 0.45$, and find evidence for mass segregation within rich groups but find no evidence for mass segregation within poor groups. Using a $V_{\rm max}$-weighted sample with a stellar mass cut at $10^{9.0}{\rm M}_{\odot}$, van den Bosch et al. (2008) find evidence for mass segregation in SDSS groups.

It is clear that there is no consensus regarding the strength of mass segregation in groups and clusters or its halo mass dependence.

In this Letter, we present evidence of the presense of a small, but significant, amount of mass segregation in SDSS galaxy groups. We show that the detection of mass segregation is dependent on stellar mass completeness, with completeness cuts at relatively high stellar masses potentially masking underlying mass segregation trends. We also show that the strength of mass segregation scales inversely with halo mass, with cluster-sized haloes showing little to no observable mass segregation. In Section 2.2, we briefly describe our data set, in Section 2.3 we present our results from this work, in Section ... we provide a discussion of our results, and in Section ... we give a summary of the results and make concluding statements.

In this Letter, we assume a flat Λ cold dark matter cosmology with $\Omega_M = 0.3$, $\Omega_\Lambda = 0.7$, and $H_0 = 70\,\mathrm{km\,s^{-1}\,Mpc^{-1}}$.

2.2 Data

The results presented in this Letter utilize the group catalogue of Yang et al. (2007). This catalogue is contructed by applying the halo-based group finder of Yang et al. (2005, 2007) to the New York University Value-Added Galaxy Catalogue (NYU-VAGC; Blanton et al. 2005b), which is based on the SDSS Data Release 7 (DR7; Abazajian et al. 2009. Stellar masses are obtained from the NYU-VAGC and are computed using the methodology of Blanton & Roweis (2007), assuming a Chabrier (2003) initial mass function. Halo masses are determined using the ranking of the characteristic stellar mass, $M_{\star,\mathrm{grp}}$, and assuming a relationship between M_{halo} and $M_{\star,\mathrm{grp}}$ (Yang et al., 2007). $M_{\star,\mathrm{grp}}$ is defined by Yang et al. as

$$M_{\star,\mathrm{grp}} = \frac{1}{g(L_{19.5},\, L_{\mathrm{lim}})} \sum_i \frac{M_{\mathrm{star},i}}{C_i}, \tag{2.1}$$

where $M_{\mathrm{star},i}$ is the stellar mass of the ith member galaxy, C_i is the completeness of the survey at the position of that galaxy, and $g(L_{19.5},\, L_{\mathrm{lim}})$ is a correction factor which accounts for galaxies missed due to the magnitude limit of the survey.

Halo-centric distance for each galaxy is not given explicitly in the Yang catalogue; however, we calculate it using the redshift of the group and the angular separation of the galaxy and halo centre on the sky. We measure group-centric radius from the luminosity-weighted centre of each group, and normalize our grou-centric radii by R_{200}. We use the definition for R_{200} as given in Carlberg et al. (1997)

$$R_{200} = \frac{\sqrt{3}\sigma}{10H(z)}, \tag{2.2}$$

where the Hubble parameter, $H(z)$, is defined as

$$H(z) = H_0\sqrt{\Omega_M(1+z)^3 + \Omega_\Lambda}, \tag{2.3}$$

and we calculate the velocity dispersion, σ, as

$$\sigma = 397.9\,\mathrm{km\,s^{-1}} \left(\frac{M_{\mathrm{halo}}}{10^{14}\,h^{-1}\mathrm{M}_\odot}\right)^{0.3214}, \tag{2.4}$$

where the above is a fitting function given in Yang et al. (2007).

For our analysis we select group galaxies with redshift, $z < 0.1$, that are within two virial radii of the group centre, and groups with a minimum of three galaxy members – although our results are not sensitive to these specific cuts. For our sample over 95 per cent of group galaxies reside within two virial radii of the group centre. We also subtract the most massive galaxy (MMG) from each group, to ensure that any underlying radial mass trend is not contaminated by the MMG.

This sample is not volume limited, therefore, the sample will suffer from the Malmquist bias. This leads to a bias towards objects of higher luminosity and stellar mass, with increasing redshift. To account for this bias we weight our sample by $1/V_{\rm max}$, where $V_{\rm max}$ is the comoving volume of the Universe out to a comoving radius at which the galaxy would have met the selection criteria for the sample. For our $V_{\rm max}$ weights we apply the values presented in the catalogue of Simard et al. (2011) to our sample.

In order to investigate the effect of stellar mass limits on the detection of mass segregation, we use samples corresponding to various stellar mass cuts. We perform our analysis on an unweighted sample with two mass cuts corresponding to $M_{\rm star} > 10^{10.5}{\rm M}_{\odot}$ (4152 galaxies in 1970 groups) and $M_{\rm star} > 10^{10.0}{\rm M}_{\odot}$ (26 774 galaxies in 4534 groups); and a $V_{\rm max}$-weighted sample with mass cuts at $M_{\rm star} > 10^{9.0}{\rm M}_{\odot}$ (56 957 galaxies in 7217 groups) and $M_{\rm star} > 10^{8.5}{\rm M}_{\odot}$ (59 791 galaxies in 7289 groups). The unweighted sample is stellar mass complete down to $M_{\rm star} > 10^{10.0}{\rm M}_{\odot}$. Therefore, for both the weighted and unweighted sample, we have two different stellar mass cuts, giving us four separate samples in total.

2.3 Results

2.3.1 Mass segregation in SDSS groups

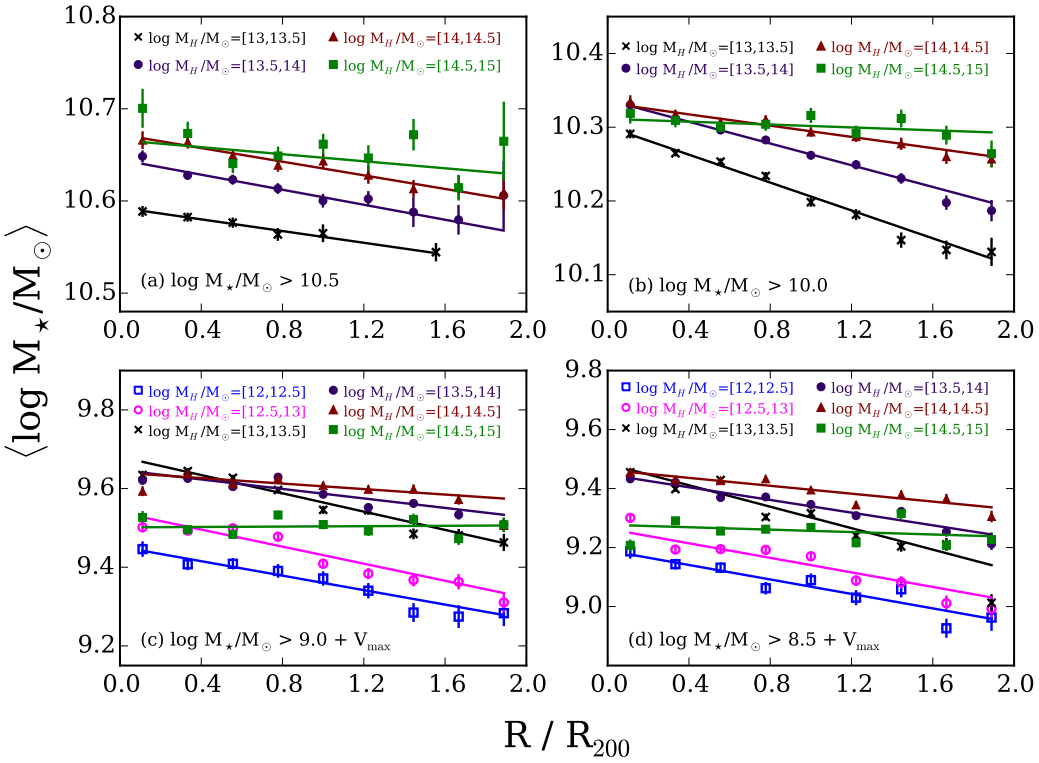

Figure 2.1 All panels show mean mass as a function of normalized distance for various halo mass bins, with error bars corresponding to 1σ statistical errors. The solid lines correspond to weighted least-squares fits for each halo mass bin. Top left: unweighted sample, for galaxies with $\log(M_{\rm star}/{\rm M}_\odot) > 10.5$. Top right: unweighted sample, for galaxies with $\log(M_{\rm star}/{\rm M}_\odot) > 10.0$. Bottom left: $V_{\rm max}$-weighted sample, for galaxies with $\log(M_{\rm star}/{\rm M}_\odot) > 9.0$. Bottom right: $V_{\rm max}$-weighted sample, for galaxies with $\log(M_{\rm star}/{\rm M}_\odot) > 8.5$. Note that different mass scales are used in each panel. There are more halo mass bins in the bottom row due to the increased number of low-mass galaxies as a result of $V_{\rm max}$ weighting.

In Fig. 2.1 we plot mean stellar mass as a function of radial distance from the group centre for various halo mass bins. Fig 2.1(a) corresponds to our

high-mass cut, unweighted sample; Fig 2.1(b) corresponds to our low-mass cut, unweighted sample; Fig 2.1(c) corresponds to our high-mass cut, weighted sample; and Fig 2.1(d) corresponds to our low-mass cut, weighted sample.

For all halo mass bins, and regardless of the mass cut, the unweighted sample shows statistically significant mass segregation with a weighted linear least-squares fit. The $V_{\rm max}$-weighted sample shows statistically significant mass segregation for the five lower halo mass bins, whereas the highest halo mass bin has a best-fitting slope consistent with zero – this trend hold for both mass cuts. For both the weighted and unweighted samples there is a clear trend of the slope with halo mass – more massive haloes show weaker mass segregation. This result will be discussed in Section ...

We find that our highest halo mass sample ($M_{\rm halo} > 10^{14.5}{\rm M}_{\odot}$) has a large number of low-mass galaxies when compared to the high-halo-mass samples, which leads to a smaller mean stellar mass in the $V_{\rm max}$-weighted results shown in Figs 2.1(c) and (d). While this introduces a shift in normalization, it does not affect the mass segregation trend and therefore does not change the key result that mass segregation depends on halo mass.

2.3.2 Massive galaxy fraction

An alternative way to investigate galaxy populations within the group sample is to study the fraction of 'massive' galaxies at various group-centric radii. In Fig..., we plot the fraction of massive galaxies as a function of radial distance for two different definitions of what constitutes a massive galaxy. We calculate the massive fraction for each radial bin as

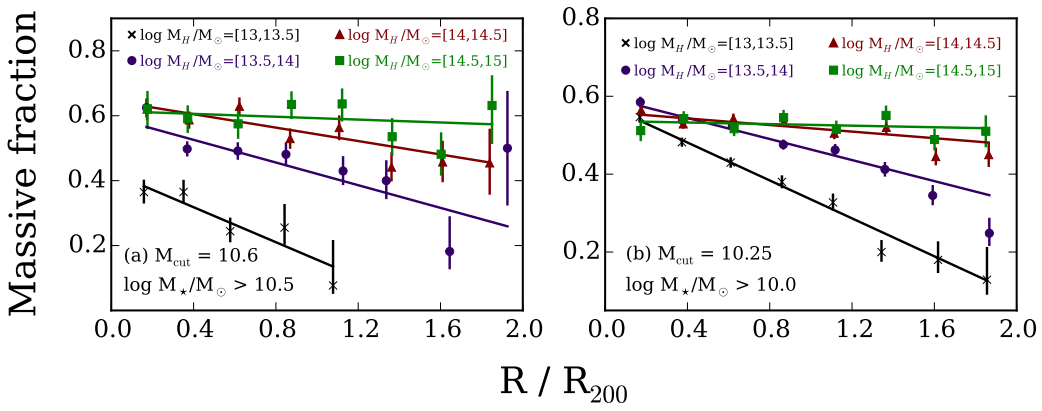

Figure 2.2 Fraction of massive galaxies with respect to normalized radial distance. Error bars are given by a 1σ binomial confidence interval, calculated using the beta distribution as outlined in Cameron (2011). The solid lines correspond to weighted least-squares fits for each halo mass bin. Left-hand panel: the fraction of galaxies with $\log(M_{\rm star}/{\rm M}_\odot) > 10.25$ as a function of radial distance, for the unweighted sample with $M_{\rm star} > 10^{10}{\rm M}_\odot$. Right-hand panel: the fraction of galaxies with $\log(M_{\rm star}/{\rm M}_\odot) > 10.5$ as a function of radial distance, for the unweighted sample with $M_{\rm star} > 10^{10}{\rm M}_\odot$.

$$f_m(M_{\rm cut}) = \frac{\#\text{ galaxies with } M_{\rm star} > M_{\rm cut}}{\#\text{ galaxies with } M_{\rm star} > 10^{10}{\rm M}_\odot}, \tag{2.5}$$

where $M_{\rm cut}$ is a stellar mass cut-off above which we define a massive galaxy. We initially apply a high-mass galaxy cut, $M_{\rm cut}$, at $10^{10.25}{\rm M}_\odot$, corresponding to the median stellar mass of the unweighted sample (with the low-mass cut at $10^{10}{\rm M}_\odot$). Comparing Figs 2.1(b) and 2.2(a) we see essentially identical trends. We observe the same trends of mass segregation whether we look at the average galaxy mass at a given radius, or consider the fraction of massive galaxies.

To confirm that this trend is robust regardless of the mass cut-off used to define a massive galaxy, we make the same plot but now use $M_{\rm cut} = 10^{10.5}{\rm M}_\odot$. Comparing Figs 2.2(a) and (b) we see that while the overall fractions of massive

galaxies decrease with increasing the stellar mass cut, the trend essentially stays the same. There is clear evidence for mass segregation and the strength of mass segregation depends on halo mass.

2.4 Discussion

2.4.1 Effect of including low-mass galaxies

The results in Fig. 2.1 show that mass segregation generally increases when lower mass galaxies are included. To quantify this effect we can compare the best-fitting slopes corresponding to the high-mass and the low-mass cut samples.

For a given halo mass, the low-mass cut sample displays larger slopes than the high-mass cut sample for two of the halo mass bins. The slopes corresponding to the other two halo mass bins are consistent with being equal. For the weighted samples we find similar results with the low-mass cut sample showing larger slopes for three of the halo mass bins, and the other three halo mass bins showing slopes consistent with being equal.

This suggests that the inclusion of low-mass galaxies has a measurable effect on the observation of mass-segregation. Studies which make mass cuts at moderate to high-stellar mass, are potentially missing a mass segregation contribution from low-mass galaxies. The observation of mild mass segregation is consistent with the low redshift sample of Ziparo et al. (2013); however, they see similar mass-radius relations regardless of the stellar mass cut applied.

2.4.2 Halo mass dependence

Figs 2.1 and 2.2 clearly indicate that the highest halo mass bins show the least mass segregation. This trend is consistent in all cases, regardless of stellar mass cut or whether the sample had $V_{\rm max}$ weights applied. Our observed dependence on halo mass is consistent with results finding no measurable mass segregation in galaxy clusters (Pracy et al., 2005; von der Linden et al., 2010; Vulcani et al., 2013)

It has been shown through N-body simulations that the dynamical friction time-scale scales with M_h/M_s (e.g. Taffoni et al., 2003; Conroy et al., 2007; Boylan-Kolchin et al., 2008), where M_s is the initial satellite mass and M_h is the mass of the host halo. For a given satellite mass, this implies a longer dynamical friction time-scale for larger haloes, which is consistent with our result. This can be interpreted as an increase in tidal stripping efficiency as M_h/M_s increases (Taffoni et al., 2003). Gan et al. (2010) have shown that for an infalling satellite the dynamical friction time-scale increases with a stronger tidal field. This is due to tidal stripping retarding the decay of satellite angular momentum, which increases the dynamical friction time-scale.

It should be noted that the merger time-scale scales with M_s/M_h Jiang et al. (2008), which implies a higher merger efficiency in low-mass haloes, for a given satellite mass. The build-up of massive objects through galaxy mergers could enhance mass segregation in low-mass haloes, in accordance with our results.

There has been evidence of cluster galaxies having their star formation quenched in lower mass groups ($\sim 10^{13}\mathrm{M}_{\odot}$) prior to accretion into the cluster

environment (e.g. Zabludoff & Mulchaey, 1998; McGee et al., 2009; De Lucia et al., 2012; Hou et al., 2014). This pre-processing could potentially provide an explanation of our observed mass segregation trends with halo mass. If mass segregation is present in the group environment as a result of pre-processing, the recent accretion of multiple pre-processed groups to form a galaxy cluster could result in little to no observed mass segregation in the cluster as a whole. In other words, if the cluster environment consists of multiple subhaloes at various cluster-centric radii, while individual subhaloes may show mass segregation, the total effect of these subhaloes together may leave the cluster with a relatively uniform radial mass distribution.

Vulcani et al. (2014) apply semi-analytic models to the Millenium Simulation (Springel et al., 2005) to study galaxy mass functions in different environments. Vulcani et al. simulate galaxy mass functions for three halo masses, $\log(M_{\rm halo}/M_{\odot}) = \{13.4, 14.1, 15.1\}$, as a function of cluster-centric radius. In the lowest mass halo they find the mass function depends slightly on cluster-centric radius, with the innermost regions showing flatter mass functions at low and intermediate masses. This trend persists, but is not as strong at intermediate halo mass. The highest halo mass bin shows virtually identical mass function shapes for all cluster-centric radii. This result is indicative of measurable mass segregation for the low- and intermediate-mass haloes, with the strength of mass segregation decreasing with increasing halo mass. These simulation trends show excellent agreement with our observed dependence of mass segregation on halo mass.

2.4.3 Reconciling previous results

In Section 2.1, we mention previous literature results which presente vidence both for and against the presence of mass segregation in groups and clusters. We argue that the majority of these results can be reconciled with our two main findings.

(i) Mass segregation is enhanced with the inclusion of low-mass galaxies in a sample.

(ii) Mass segregation decreases with increasing halo mass, with high-mass haloes showing little to no mass segregation.

Of the studies mentioned in Section 2.1, those which observe no evidence for mass segregation either: make a mass completeness cut at intermediate to high stellar mass, or observe this lack of mass segregation only in high-mass haloes. Therefore, the lack of observed mass segregation can potentially be explained through the lack of low-mass galaxies in the study survey, or the study being limited to high-halo-mass environments.

2.5 Conclusion

In this Letter, we examine mass segregation trends in the Yang et al. (2007) SDSS DR7 groups for various stellar and halo mass cuts. WE show that a small, but significant, amount of mass segregation is present in these groups. This mass segregation shows consistent trends, with lower stellar mass samples showing stronger mass segregation, and galaxies in large haloes showing little to no mass segregation.

The magnitude of mass segregation we measure, especially in high-mass haloes, is potentially indicative of dynamical friction not acting efficiently. We discuss previous literature to provide possible explanations for the observed trends, showing that our observed trends with halo mass agree with prior results. Further work with hydrodynamic simulations would be helpful to further constrain the important mechanisms responsible for our observed mass trends and the lack of mass segregation in high-mass haloes.

2.6 Acknowledgements

We thank the anonymous referee for their various helpful comments and suggestions. IDR and LCP thank the National Science and Engineering Research Council of Canada for funding. We thank X. Yang et al. for making their SDSS DR7 group catalogue public, L. Simard et al. for the publication of their SDSS DR7 morphology catalogue, and the NYU-VAGC team for the publication of their SDSS DR7 catalogue. This research would not have been possible without these public catalogues.

Funding for the SDSS has been provided by the Alfred P. Sloan Foundation, the Participating Institutions, the National Science Foundation, the US Department of Energy, the National Aeronautics and Space Administration, the Japanese Monbukagakusho, the Max Planck Society, and the Higher Education Funding Council for England. The SDSS website is http://www.sdss.org/.

Bibliography

Abazajian, K. N., Adelman-McCarthy, J. K., Agüeros, M. A., Allam, S. S., Allende Prieto, C., An, D., Anderson, K. S. J., Anderson, S. F., Annis, J., Bahcall, N. A., & et al. 2009, ApJS, 182, 543

Ball, N. M., Loveday, J., & Brunner, R. J. 2008, MNRAS, 383, 907

Balogh, M. L., McGee, S. L., Mok, A., Wilman, D. J., Finoguenov, A., Bower, R. G., Mulchaey, J. S., Parker, L. C., & Tanaka, M. 2014, MNRAS, 443, 2679

Balogh, M. L., Navarro, J. F., & Morris, S. L. 2000, ApJ, 540, 113

Blanton, M. R., Eisenstein, D., Hogg, D. W., Schlegel, D. J., & Brinkmann, J. 2005a, ApJ, 629, 143

Blanton, M. R. & Roweis, S. 2007, AJ, 133, 734

Blanton, M. R., Schlegel, D. J., Strauss, M. A., Brinkmann, J., Finkbeiner, D., Fukugita, M., Gunn, J. E., Hogg, D. W., Ivezić, Ž., Knapp, G. R., Lupton, R. H., Munn, J. A., Schneider, D. P., Tegmark, M., & Zehavi, I. 2005b, AJ, 129, 2562

Boylan-Kolchin, M., Ma, C.-P., & Quataert, E. 2008, MNRAS, 383, 93

Brough, S., Forbes, D. A., Kilborn, V. A., & Couch, W. 2006, MNRAS, 370, 1223

Cameron, E. 2011, PASA, 28, 128

Carlberg, R. G., Yee, H. K. C., Ellingson, E., Morris, S. L., Abraham, R., Gravel, P., Pritchet, C. J., Smecker-Hane, T., Hartwick, F. D. A., Hesser, J. E., Hutchings, J. B., & Oke, J. B. 1997, ApJ, 485, L13

Chabrier, G. 2003, PASP, 115, 763

Chandrasekhar, S. 1943, ApJ, 97, 255

Conroy, C., Ho, S., & White, M. 2007, MNRAS, 379, 1491

De Lucia, G., Weinmann, S., Poggianti, B. M., Aragón-Salamanca, A., & Zaritsky, D. 2012, MNRAS, 423, 1277

Eke, V. R., Baugh, C. M., Cole, S., Frenk, C. S., King, H. M., & Peacock, J. A. 2005, MNRAS, 362, 1233

Gan, J.-L., Kang, X., Hou, J.-L., & Chang, R.-X. 2010, Research in Astronomy and Astrophysics, 10, 1242

Geller, M. J. & Huchra, J. P. 1983, ApJS, 52, 61

Hogg, D. W., Blanton, M. R., Brinchmann, J., Eisenstein, D. J., Schlegel, D. J., Gunn, J. E., McKay, T. A., Rix, H.-W., Bahcall, N. A., Brinkmann, J., & Meiksin, A. 2004, ApJ, 601, L29

Hou, A., Parker, L. C., & Harris, W. E. 2014, MNRAS, 442, 406

Jiang, C. Y., Jing, Y. P., Faltenbacher, A., Lin, W. P., & Li, C. 2008, ApJ, 675, 1095

McGee, S. L., Balogh, M. L., Bower, R. G., Font, A. S., & McCarthy, I. G. 2009, MNRAS, 400, 937

Oemler, Jr., A. 1974, ApJ, 194, 1

Poggianti, B. M., Desai, V., Finn, R., Bamford, S., De Lucia, G., Varela, J., Aragón-Salamanca, A., Halliday, C., Noll, S., Saglia, R., Zaritsky, D., Best, P., Clowe, D., Milvang-Jensen, B., Jablonka, P., Pelló, R., Rudnick, G., Simard, L., von der Linden, A., & White, S. 2008, ApJ, 684, 888

Pracy, M. B., Driver, S. P., De Propris, R., Couch, W. J., & Nulsen, P. E. J. 2005, MNRAS, 364, 1147

Presotto, V., Iovino, A., Scodeggio, M., Cucciati, O., Knobel, C., Bolzonella, M., Oesch, P., Finoguenov, A., Tanaka, M., Kovač, K., Peng, Y., Zamorani, G., Bardelli, S., Pozzetti, L., Kampczyk, P., López-Sanjuan, C., Vergani, D., Zucca, E., Tasca, L. A. M., Carollo, C. M., Contini, T., Kneib, J.-P., Le Fèvre, O., Lilly, S., Mainieri, V., Renzini, A., Bongiorno, A., Caputi, K., de la Torre, S., de Ravel, L., Franzetti, P., Garilli, B., Lamareille, F., Le Borgne, J.-F., Le Brun, V., Maier, C., Mignoli, M., Pellò, R., Perez-Montero, E., Ricciardelli, E., Silverman, J. D., Tresse, L., Barnes, L., Bordoloi, R., Cappi, A., Cimatti, A., Coppa, G., Koekemoer, A. M., McCracken, H. J., Moresco, M., Nair, P., & Welikala, N. 2012, A&A, 539, A55

Simard, L., Mendel, J. T., Patton, D. R., Ellison, S. L., & McConnachie, A. W. 2011, ApJS, 196, 11

Springel, V., White, S. D. M., Jenkins, A., Frenk, C. S., Yoshida, N., Gao, L., Navarro, J., Thacker, R., Croton, D., Helly, J., Peacock, J. A., Cole,

S., Thomas, P., Couchman, H., Evrard, A., Colberg, J., & Pearce, F. 2005, Nature, 435, 629

Taffoni, G., Mayer, L., Colpi, M., & Governato, F. 2003, MNRAS, 341, 434

Tal, T., Dekel, A., Oesch, P., Muzzin, A., Brammer, G. B., van Dokkum, P. G., Franx, M., Illingworth, G. D., Leja, J., Magee, D., Marchesini, D., Momcheva, I., Nelson, E. J., Patel, S. G., Quadri, R. F., Rix, H.-W., Skelton, R. E., Wake, D. A., & Whitaker, K. E. 2014, ApJ, 789, 164

van den Bosch, F. C., Pasquali, A., Yang, X., Mo, H. J., Weinmann, S., McIntosh, D. H., & Aquino, D. 2008, ArXiv e-prints

von der Linden, A., Wild, V., Kauffmann, G., White, S. D. M., & Weinmann, S. 2010, MNRAS, 404, 1231

Vulcani, B., De Lucia, G., Poggianti, B. M., Bundy, K., More, S., & Calvi, R. 2014, ApJ, 788, 57

Vulcani, B., Poggianti, B. M., Oemler, A., Dressler, A., Aragón-Salamanca, A., De Lucia, G., Moretti, A., Gladders, M., Abramson, L., & Halliday, C. 2013, A&A, 550, A58

Wetzel, A. R., Tinker, J. L., & Conroy, C. 2012, MNRAS, 424, 232

Wetzel, A. R., Tinker, J. L., Conroy, C., & van den Bosch, F. C. 2013, MNRAS, 432, 336

Yang, X., Mo, H. J., van den Bosch, F. C., & Jing, Y. P. 2005, MNRAS, 356, 1293

Yang, X., Mo, H. J., van den Bosch, F. C., Pasquali, A., Li, C., & Barden, M. 2007, ApJ, 671, 153

Zabludoff, A. I. & Mulchaey, J. S. 1998, ApJ, 496, 39

Ziparo, F., Popesso, P., Biviano, A., Finoguenov, A., Wuyts, S., Wilman, D., Salvato, M., Tanaka, M., Ilbert, O., Nandra, K., Lutz, D., Elbaz, D., Dickinson, M., Altieri, B., Aussel, H., Berta, S., Cimatti, A., Fadda, D., Genzel, R., Le Flo'ch, E., Magnelli, B., Nordon, R., Poglitsch, A., Pozzi, F., Portal, M. S., Tacconi, L., Bauer, F. E., Brandt, W. N., Cappelluti, N., Cooper, M. C., & Mulchaey, J. S. 2013, MNRAS, 434, 3089

Chapter 3

Comparing galaxy morphology and star formation properties in X-ray bright and faint groups and cluster

3.1 Introduction

Numerous studies have shown a strong environmental dependence on the star-forming and morphological properties of galaxies (e.g. Butcher & Oemler, 1978; Dressler, 1980; Postman & Geller, 1984; Dressler et al., 1999; Blanton et al., 2005a; Wetzel et al., 2012). Low-density regimes tend to be dominated by star-forming, late-type galaxies whereas high-density areas, such as galaxy clusters, tend to be primarily populated by quiescent, early-type galaxies. Within individual clusters, galaxy morphologies tend to distribute as a function of local density (or equivalently cluster-centric radius), with high fractions of late-type galaxies being found at large radii and the regions near the cluster core being dominated by early-types (e.g. Dressler, 1980; Postman & Geller, 1984; Postman et al., 2005). This effect has become known as the morphology-

density relation. While galaxies tends to distribute based on their star-forming and morphological properties, the mechanism(s) responsible for the quenching of star formation and morphological transformations in galaxies are not well constrained – although many have been proposed. Both mergers and impulsive galaxy-galaxy interactions ('harassment') (e.g. Moore et al., 1996) can induce starburst events in galaxies leading to rapid consumption of gas reserves and star formation quenching. Within the virial radius of a group or cluster the stripping of gas from galaxies becomes efficient. Both the stripping of hot halo gas ('strangulation') (e.g. Kawata & Mulchaey, 2008) and cold gas stripping due to a dense intracluster medium ('ram-pressure') (e.g. Gunn & Gott, 1972) can quench star formation. As well, tidal interactions can affect gas reservoirs by transporting gas from the galactic halo outwards which subsequently allows it to more easily be stripped from the galaxy (Chung et al., 2007).

On top of these environmental quenching mechanisms, previous authors have found that secular processes, which depend on galaxy mass, appear to play a significant role in star formation quenching (Balogh et al., 2004; Muzzin et al., 2012). The emergent picture for star formation quenching appears to be some combination of environmental quenching mechanisms and internal, secular processes. In particular, (Peng et al., 2010) suggests that in the low-redshift Universe, environmental quenching is dominant for galaxies with $M_\star \lesssim 10^{10.5}\mathrm{M}_\odot$, whereas for galaxies with $M_\star \gtrsim 10^{10.5}\mathrm{M}_\odot$ mass quenching plays the more important role.

While environmental and mass quenching within individual haloes are seemingly strong effects, it is important to realize that groups and clusters are

not isolated structures. In particular, galaxies can be pre-quenched in group haloes prior to infall into a larger cluster. This 'pre-processing' suggests that many galaxies may already be quenched upon cluster infall. Simulations have shown that between $\sim$ 25 and 45 per cent of infalling cluster galaxies may have been pre-processed (McGee et al., 2009; De Lucia et al., 2012). Observationally, (Hou et al., 2014) find that $\sim$ 25 per cent fo the infall population reside in subhaloes for massive clusters ($M_H \gtrsim 10^{14.5}\mathrm{M}_\odot$). This pre-quenching of galaxies in groups could potentially be driven by galaxy interactions and mergers which are favoured in the group regime as a result of lower relative velocities between member galaxies (Barnes, 1985; Brough et al., 2006).

An important method for study the quenching mechanisms in groups and clusters is to study the dependence of the star formation and morphological properties of galaxies on the conditions of their host halo (e.g. halo mass, X-ray luminosity, etc.). In particular, if quenching mechanisms depend on the density of the intra-group/cluster medium (IGM/ICM) – for example, ram-pressure stripping of cold gas – then one would expect to see galaxy populations which are preferentially passive in haloes with high X-ray luminosities. Such correlations have been looked for in previous studies, primarily within cluster environments.

In particular, Ellingson et al. (2001) find no positive correlation between the fraction of old galaxies and X-ray gas density. Balogh et al. (2002a) conclude that the level of star formation found in their 'low-L_X' sample is consistent with the levels seen in their CNOC1 sample consisting of higher mass clusters. Fairley et al. (2002) and Wake et al. (2005) both study the fractions of blue

galaxies at intermediate redshifts and find no discernible trend between blue fraction and X-ray luminosity. Using multivariate regression Popesso et al. (2007b) find that cluster star formation depends on cluster richness but find no additional dependence on X-ray luminosity. In addition, they find no significant correlation between star-forming fraction and any global cluster property (M_{200}, σ_v, $N_{\rm gal}$, and L_X). Lopes et al. (2014) find no dependence of blue fraction on X-ray luminosity and the only slight dependence they find between disc fraction and X-ray luminosity is within the central and most dense regions.

Conversely, Balogh et al. (2002b) find that galaxies in their 'low-L_X' sample have preferentially high disc fractions compared to galaxies in their 'high-L_X' sample. Postman et al. (2005) find that the bulge-dominated fraction for galaxies in high X-ray luminosity clusters is higher than for those in low X-ray luminosity clusters. In contrast with their star formation results, Popesso et al. (2007b) do find a significant anticorrelation between blue fraction and X-ray luminosity. Finally, Urquhart et al. (2010) find an anticorrelation between blue fraction and X-ray temperature for galaxies in intermediate redshift clusters.

In this paper we revisit the dependence of galaxy star formation and morphological properties on the X-ray luminosity of the host halo. Specifically, as a result of the large SDSS X-ray sample presented in Wang et al. (2014), we are able to control for stellar mass, halo mass, and radial dependences through fine-binning of the data set. This allows us to more directly investigate the effect of X-ray luminosity on galaxies in different environments.

The results of this study are presented as follows. In Section 3.2 we briefly describe the SDSS group catalogues utilized in this work, as well as the star

formation and morphology catalogues which we match to the group data set. In Section 3.3 we present the primary results of this paper, specifically, the differences between star-forming and morphological trends in environments with different X-ray luminosities. In Section 3.4 we provide a discussion of the results presented in this paper. Finally, in Section 3.5 we provide a summary of the key results and make concluding statements.

In this paper we assume a Λ cold dark matter cosmology with $\Omega_M = 0.3$, $\Omega_\Lambda = 0.7$, and $H_0 = 70\,\mathrm{km\,s^{-1}\,Mpc^{-1}}$.

3.2 Data

3.2.1 Yang group catalogue

This work relies heavily on the group catalogue of Yang et al. (2007). The Yang group catalogue is constructed by applying the iterative halo-based group finder of Yang et al. (2005, 2007) to the New York University Value-Added Galaxy Catalogue (NYU-VAGC; Blanton et al. 2005b), which is based on the Sloan Digital Sky Survey Data Release 7 (SDSS-DR7; Abazajian et al. 2009). The Yang group catalogue has a wide range of halo masses, spanning from $\sim 10^{12}\mathrm{M}_\odot$ to $\sim 10^{15}\mathrm{M}_\odot$. The catalogue contains both objects which would be classified as groups ($10^{12} \lesssim M_H \lesssim 10^{14}$) and as clusters ($M_H \gtrsim 10^{14}\mathrm{M}_\odot$), however for brevity we will refer to all systems as groups regardless of mass.

Groups are initially populated using the traditional friends-of-friends (FOF) algorithm (e.g. Huchra & Geller, 1982), as well as assigning galaxies not yet

linked to FOF groups as the centres of potential groups. Next, the characteristic luminosity, $L_{19.5}$, defined as the combined luminosity of all group members with ${}^{0.1}M_r - 5\log h \leq -19.5$, is calculated for each group. Using the value of $L_{19.5}$ along with an assumption for the group mass-to-light ratio, $M_H/L_{19.5}$, a tentative halo mass is assigned on a group-by-group basis. The tentative halo mass is used to calculate a virial radius and velocity dispersion for each group, which are then used to add or remove galaxies from the system. Galaxies are assigned to groups under the assumption that the distribution of galaxies in phase space follows that of dark matter particles – the distribution of which is assumed to follow a spherical NFW profile (Navarro et al., 1997). This process is iterated until the group memberships no longer change.

Final halo masses given in the Yang group catalogue are determined using the ranking of the characteristic stellar mass, $M_{\star,\mathrm{grp}}$, and assuming a relationship between M_H and $M_{\star,\mathrm{grp}}$ (Yang et al., 2007). $M_{\star,\mathrm{grp}}$ is defined by Yang et al. as

$$M_{\star,\mathrm{grp}} = \frac{1}{g(L_{19.5},\, L_{\mathrm{lim}})} \sum_i \frac{M_{\star,i}}{C_i}, \tag{3.1}$$

where $M_{\star,i}$ is the stellar mass of the ith member galaxy, C_i is the completeness of the survey at the position of that galaxy, and $g(L_{19.5},\, L_{\mathrm{lim}})$ is a correction factor which accounts for galaxies missed due to the magnitude limit of the survey. The statistical error in M_H is on the order of 0.3 dex and mostly independent of halo mass (Yang et al., 2007).

3.2.2 SDSS X-ray catalogue

To study the X-ray properties of the group sample, we utilize the SDSS X-ray catalogue of Wang et al. (2014), which combines ROSAT All Sky Survey (RASS) X-ray images in conjunction with optical groups identified from SDSS-DR7 (Yang et al., 2007) to estimate X-ray luminosities around $\sim 65\,000$ spectroscopic groups.

To identify X-ray luminosities for individual groups, the algorithm of Shen et al. (2008) is employed. Beginning from an optical group, the most massive galaxies (MMGs) of that group are identifed – up to four MMGs are kept. The RASS field in which the MMGs reside are then identified, and an X-ray source catalogue is generated in the $0.5-2.0\,\mathrm{keV}$ band (Wang et al., 2014). The maximum X-ray emission density point is used to identify the X-ray centre of the group, and any X-ray sources not associated with the group (e.g. point source quasars or stellar object cross-matched from RASS and SDSS-DR7), within one virial radius , are masked out. Values for the X-ray background, centred on the X-ray centre, are determined and subtracted off and the X-ray luminosity, L_X, is calculated by integrating the source count profile within the X-ray radius.

Determining X-ray luminosities in this manner is susceptible to 'source confusion'. Due to projection it is possible for more than one group to contribute to the X-ray emission within the X-ray radius, leading to an overestimation of the X-ray luminosity for a given group. To account for this effect Wang et al. (2014) calculate the 'expected' average X-ray flux, $F_{X,i}$, for each group using the average $L_X - M_H$ relation taken from Mantz et al. (2010). They then cal-

culate the sum of the expected fluxes from each group for multigroup systems and determine the contribution fraction, $f_{\mathrm{mult},i}$, for each group defined as

$$f_{\mathrm{mult},i} = F_{X,i}/\Sigma_i F_{X,i}. \tag{3.2}$$

The contribution factor will approximate the fraction of the observed X-ray luminosity intrinsic to the individual group in question, therefore applying this fraction to each group will act to debias the measured X-ray luminosity from source confusion contamination.

Within the Wang catalogue 817 groups have S/N > 3, compared to the total of 34 522 groups with positive detections (positive count rates after background subtraction) and S/N > 0. We run our analysis for groups with S/N > 3 as well as groups with S/N > 0 and find that our choice of signal-to-noise cut does not change the trends that we observe, therefore we focus on the total sample (S/N > 0) to ensure a sample size which is large enough to finely bin the data in various properties simultaneously.

3.2.3 Final data set

To obtain the final data set, we match the Wang SDSS X-ray catalogue to the Yang SDSS group catalogue, giving us both optical and X-ray group properties for the sample. To obtain individual galaxy properties we further match the data set to various public SDSS catalogues as follows.

We utilize stellar masses given in the NYU-VAGC, which are computed following the methodology of Blanton & Roweis (2007).

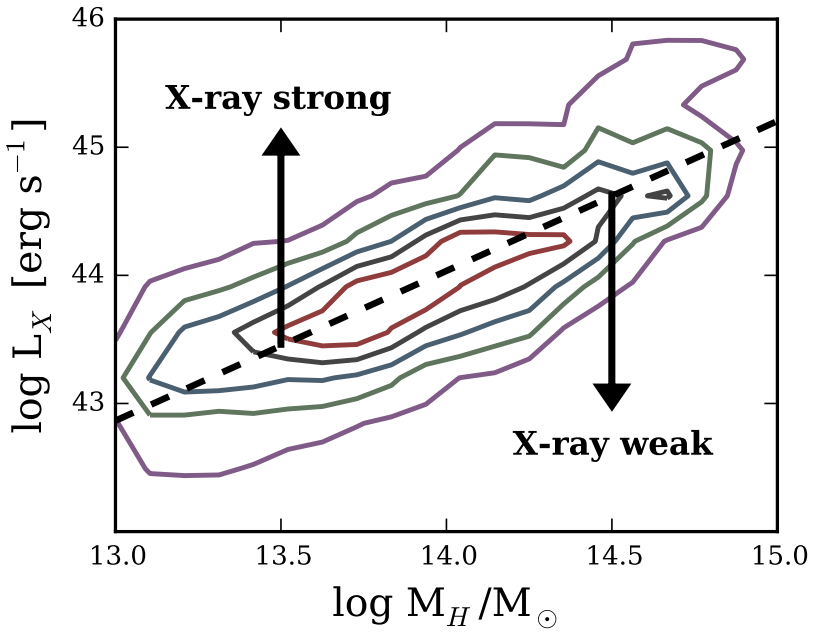

Figure 3.1 Density contours for log X-ray luminosity versus log halo mass. Dashed line corresponds to the linear least-squares best-fitting relationship.

To obtain star formation rates (SFRs) and specific star formation rates (SSFR = SFR/$M_\star$) we match the catalogue of Brinchmann et al. (2004) to the sample. SFRs given by Brinchmann et al. are determined using emission line fluxes whenever possible; however, in the case of no clear emission lines or contamination from active galactic nuclei (AGNs), SFRs are determined using the strength of the 4000 Å break (D_n4000) (Brinchmann et al., 2004).

We obtain galaxy morphologies from the catalogue of Simard et al. (2011). Simard et al. perform two-dimensional bulge + disc decompositions for over one million galaxies from the Legacy area of the SDSS-DR7, using three different fitting models: a pure Sérsic model, a bulge + disc model with a de Vaucouleurs ($n_b = 4$) bulge, and a bulge + disc model with a free n_b. To

distinguish between discy and elliptical galaxies we utilize the galaxy Sérsic index, n_g, from the pure Sérsic decomposition. We also use the $V_{\max}$ weights given by Simard et al. to correct for the incompleteness of our sample.

We calculate group-centric distances for each galaxy using the redshift of the group and the angular separation between the galaxy and the luminosity-weighted centre of its host group. We normalize all of the galaxy radii by the virial radius of the host group, R_{180}, which we calculate as in Yang et al. (2007)

$$R_{180} = 1.26\, h^{-1}\,\mathrm{Mpc} \left(\frac{M_H}{10^{14}\, h^{-1}\,\mathrm{M}_\odot} \right)^{1/3} (1+z_g)^{-1}, \tag{3.3}$$

where z_g is the redshift of the group centre.

The final data set includes groups with halo masses ranging between $10^{13} - 10^{15}\,\mathrm{M}_\odot$, and galaxies with stellar masses ranging from $10^9 - 10^{11.3}\,\mathrm{M}_\odot$. Group X-ray luminosities in the data set are between $10^{39.6} - 10^{46.4}\,\mathrm{erg\,s^{-1}}$, with a median value of $10^{43.9}\,\mathrm{erg\,s^{-1}}$, and are strongly correlated with halo mass (see Fig. 3.1). We do not make an explicit radial cut, however over 99 per cent of member galaxies fall within 1.5 virial radii. Our final sample contains 3 902 low-redshift ($z < 0.1$) groups hosting 41 173 galaxies. The catalogue of Wang et al. (2014) contains $\sim 35\,000$ groups. The fact that the final sample in this work is significantly smaller than the original catalogue is twofold. First, we restrict our sample to redshifts smaller than 0.1 which reduces the number of groups from $\sim 35\,000$ at $z < 0.2$ to $\sim 18\,000$ at $z < 0.1$. The second important cut is that we require $10^{13} < M_H < 10^{15}\mathrm{M}_\odot$ and a number of groups in the Wang catalogue have halo masses, $M_H < 10^{13}\mathrm{M}_\odot$ (where halo masses have been obtained from the catalogue of Yang et al. 2007). This cut reduces the

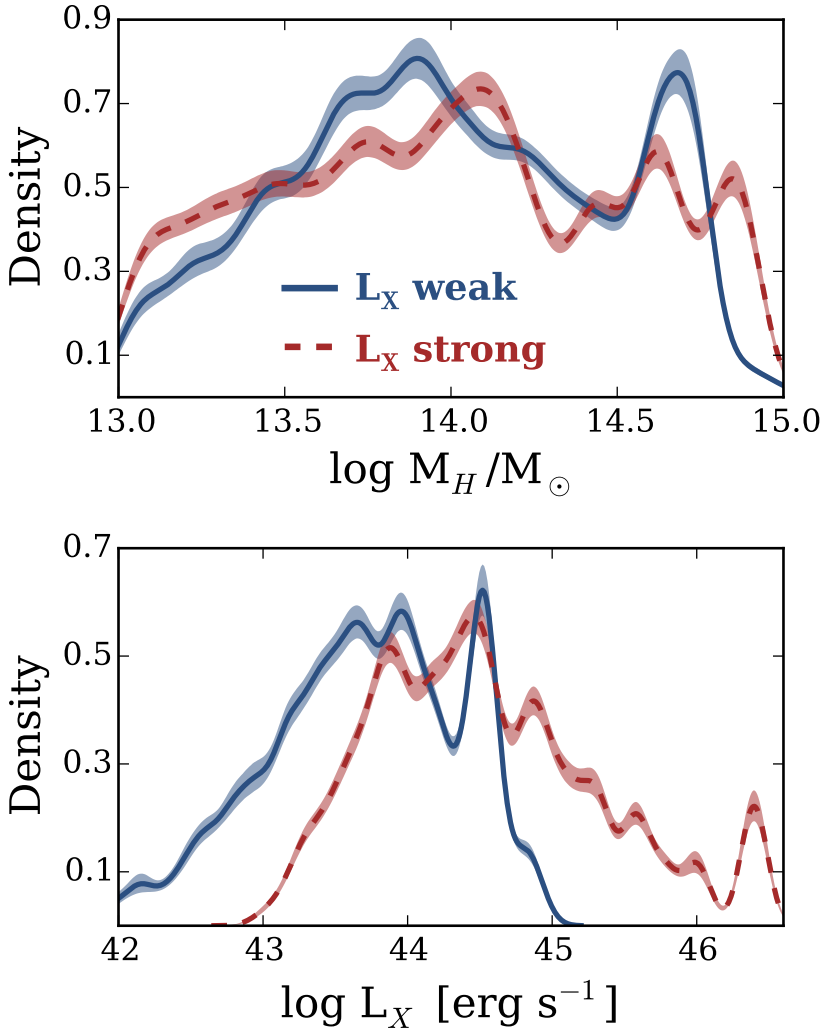

Figure 3.2 Smoothed distributions for halo mass and X-ray luminosity within the sample. Distributions are shown for both the X-ray strong (red, dashed) and the X-ray weak (blue, solid) samples. Shaded regions correspond to 2σ confidence intervals obtained from random bootstrap resampling.

remaining number of groups from $\sim$ 18 000 to $\sim$ 3 900. It should be noted that the majority of the $M_H < 10^{13}\mathrm{M}_\odot$ groups removed from the data set are groups with very low membership.

To determine the effect of X-ray luminosity on star formation and morphology we consider two X-ray luminosity samples for the majority of our analysis, which we refer to as the X-ray weak (XRW) and X-ray strong (XRS) samples. Similar to Wang et al. (2014), we define the XRS sample to consist of all galaxies found below the $\log M_H - \log L_X$ trend line. This leads to an approximately equal number of galaxies within the XRW and XRS samples. We also performed our analysis with a cut between the two X-ray samples at the median X-ray luminosity of the data set, as well as defining the two samples using the first and the fourth quartiles, however these alternative definitions of the two X-ray samples do not change the trends that we observe.

Smoothed distributions for halo mass and X-ray luminosity are shown in Fig. 3.2 for both X-ray luminosity samples. Density distributions are calculated using the `density` {`stats`} function in the statistical computing language R (R Core Team, 2013)[1] using a Gaussian kernel.

We study the dependence of star formation rates and morphology on stellar mass by binning the data by stellar mass and calculating the disc and star-forming fractions for each bin. Binning by stellar mass is important to account for the systematic dependence of star formation and morphology on stellar mass (e.g. Brinchmann et al., 2004; Whitaker et al., 2012). Additionally, as the relative balance between environmental and mass quenching is not well

[1] http://www.R-project.org/

understood, it is important to investigate the effects of environment at a given stellar mass.

We define the star-forming fraction, f_{SF}, as the fraction of galaxies in each bin with $\log \mathrm{SSFR} > -11$. Wetzel et al. (2012) show that at low redshift the division between the red sequence and the blue cloud is found at $\log \mathrm{SSFR} \simeq -11$ across a wide range of halo masses. For each stellar mass bin the star-forming fraction is given by

$$f_{SF} = \frac{V_{\max} \text{ weighted no. of galaxies with } \log \mathrm{SSFR} > -11}{V_{\max} \text{ weighted total no. of galaxies}} \tag{3.4}$$

Similarly we define the disc fraction, f_D, as the fraction of galaxies in each bin with Sérsic index, $n < 1.5$. For each stellar mass bin this is given by

$$f_{SF} = \frac{V_{\max} \text{ weighted no. of galaxies with } n < 1.5}{V_{\max} \text{ weighted total no. of galaxies}} \tag{3.5}$$

We also ran our analysis using a dividing cut at Sérsic indices of $n = 1.0$ and $n = 2.0$ to define a disc galaxy, however using these alternative definitions for a disc galaxy does not alter the trends that we observe.

3.3 Results

3.3.1 Star-forming and morphology trends in strong and weak L_X samples

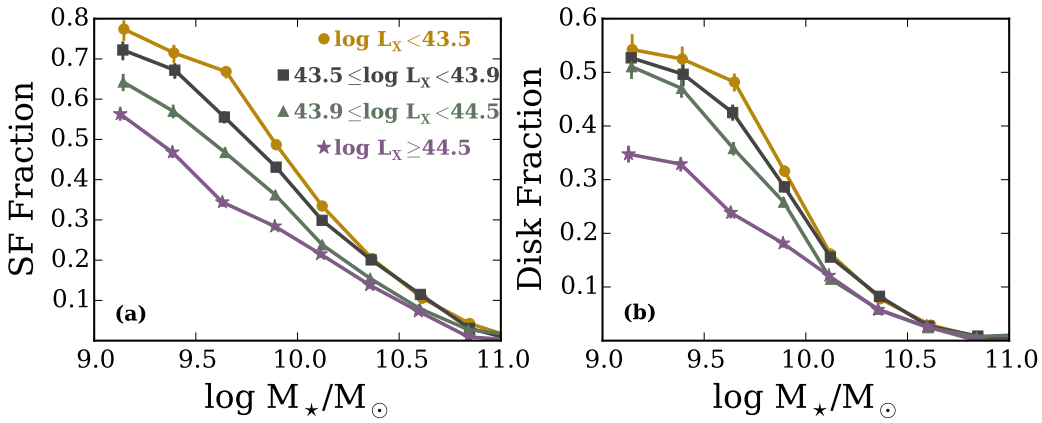

Figure 3.3 Left: star-forming fraction versus stellar mass for the four X-ray luminosity quartiles of the data sample. Right: disc fraction versus stellar mass for the four X-ray luminosity quartiles of the sample. Error bars correspond to 1σ Bayesian binomial confidence intervals given in Cameron (2011)

To investigate the effect of X-ray luminosity on galaxy properties, in Fig. 3.3 we show star-forming and disc fractions, as a function of stellar mass, for sub-samples corresponding to the four X-ray luminosity quartiles of the data set. Examination of Figs 3.3(a) and (b) show that star-forming and disc fractions follow a consistent marching order with respect to X-ray luminosity. The disc and star-forming fractions decrease as X-ray luminosity increases.

We note that the results in Fig. 3.3 consider all halo masses in the sample, however it has been found that galaxy morphology and star formation depend on local density and halo mass (Dressler, 1980; Balogh et al., 2004; Wetzel et al., 2012; Lackner & Gunn, 2013) (however also see: De Lucia et al. 2012; Hoyle et al. 2012; Hou et al. 2013). As shown in Fig. 3.1 the data show a strong correlation between X-ray luminosity and halo mass, therefore we must determine if differences shown in Fig. 3.3 are simply a result of galaxies in higher L_X environments being housed in preferentially high-mass haloes.

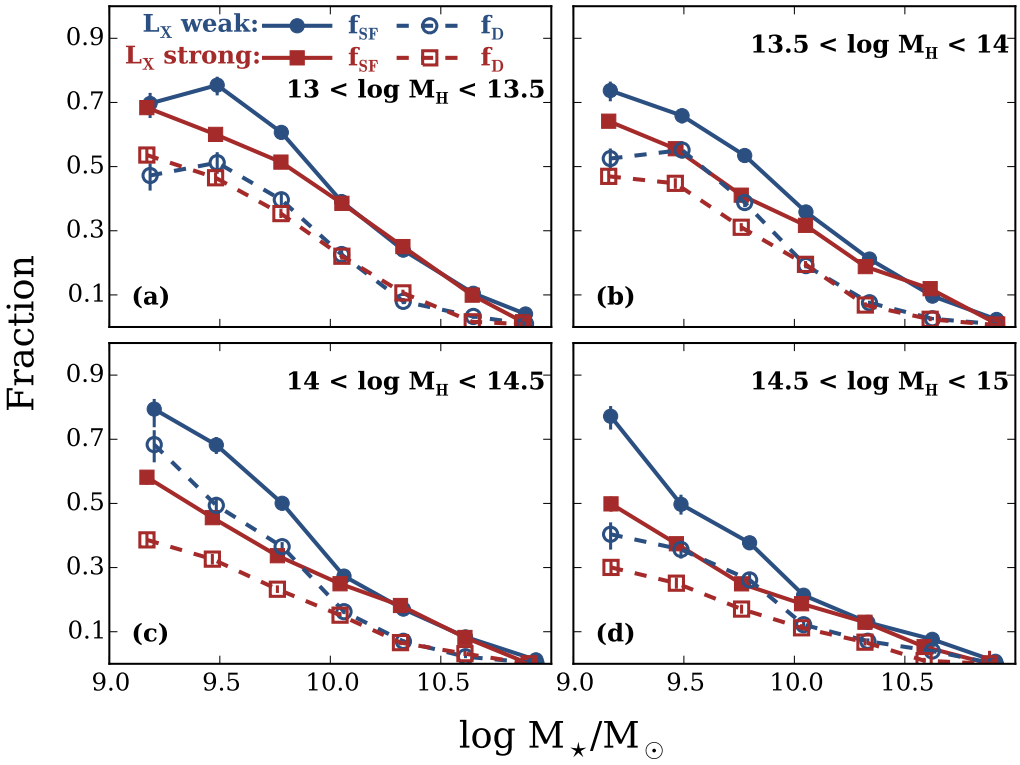

Figure 3.4 Star-forming (solid lines) and disc (dashed lines) fractions versus stellar mass, for different halo mass bins and the XRW (blue) and XRS (red) samples. Error bars correspond to 1σ Bayesian binomial confidence intervals given in Cameron (2011)

To control for any potential halo mass effect, we further bin the data into narrow halo mass bins and re-examine the dependence of galaxy properties on X-ray luminosity, considering now the XRW and XRS samples form Fig. 3.1. Fig. 3.4 shows star-forming (solid) and disc (dashed) fractions as a function of stellar mass for four different halo mass bins – ranging from 10^{13} to $10^{15}\mathrm{M}_{\odot}$ with bin widths of 0.5 dex. Data are binned according to stellar mass and markers are plotted at the median bin values. For each halo mass bin we show star-forming and disc fractions from the X-ray strong and X-ray weak samples.

For both star-forming and disc fractions we continue to see a residual trend with X-ray luminosity, even after controlling for any halo mass dependence: star-forming and disc fractions are systematically higher in the XRW sample. We see the strongest trends in the intermediate and high-mass haloes. The difference between the strong (red) and weak (blue) X-ray luminosity samples is clearest at low stellar mass, and in all haloes the two samples converge at moderate to high stellar mass.

3.3.2 Radial dependence of star-forming and morphology trends

Within host groups X-ray emission is concentrated at relatively small group-centric radii, with X-ray emission generally extending out to half a virial radius (Wang et al., 2014). If the trends we are observing are a result of increased gas density, we would expect to see enhanced trends (i.e. a larger difference between the XRS and XRW samples) at small group-centric radii and suppressed trends at large radii. To test this we further divide the data into subsets corresponding to those galaxies that lie within the X-ray emission radius (using

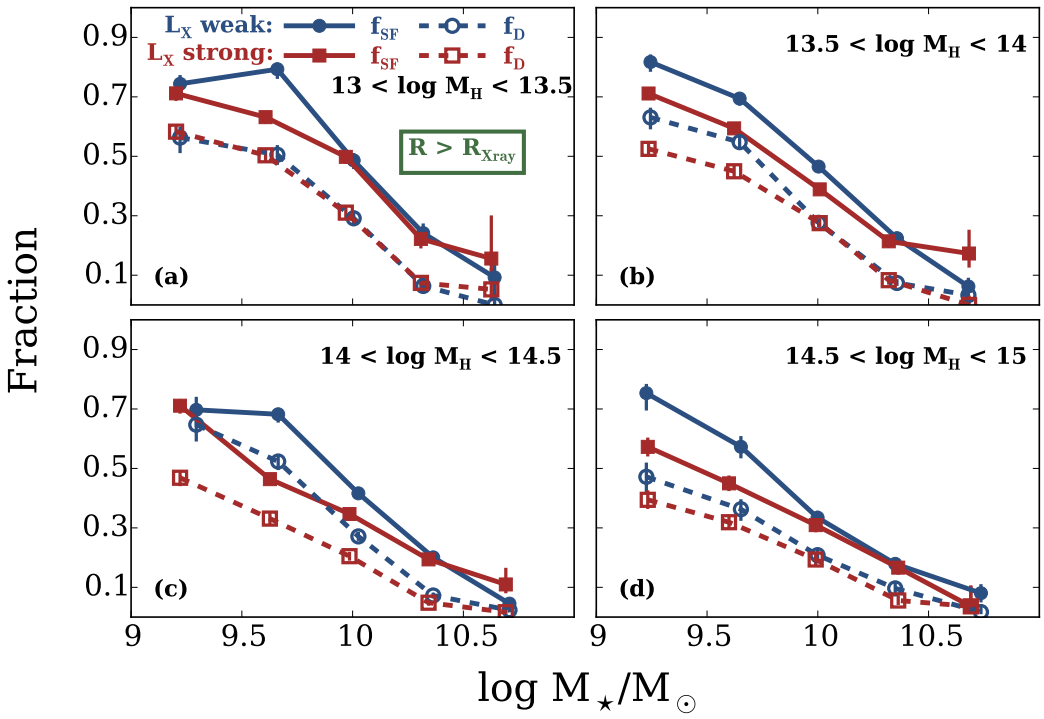

Figure 3.5 Star-forming (solid lines) and disc (dashed lines) fractions versus stellar mass, for galaxies outside of their host X-ray radius and for different halo mass bins and the two L_X samples. Error bars correspond to 1σ Bayesian binomial confidence intervals given in Cameron (2011)

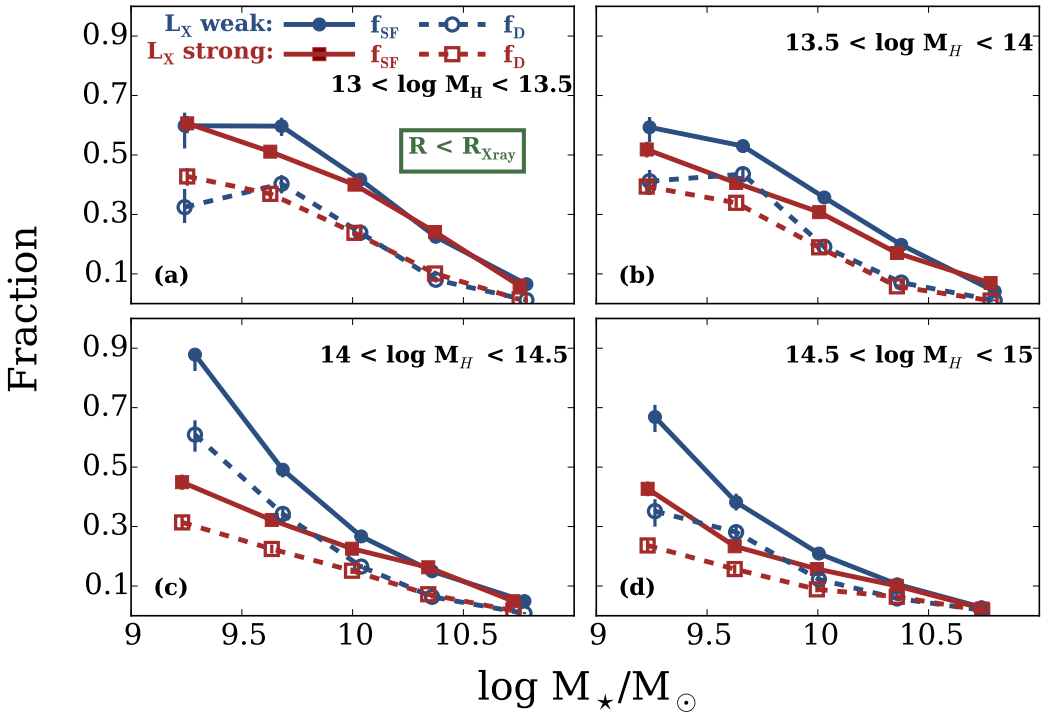

Figure 3.6 Same as Fig. 3.5 for galaxies inside of their host X-ray radius.

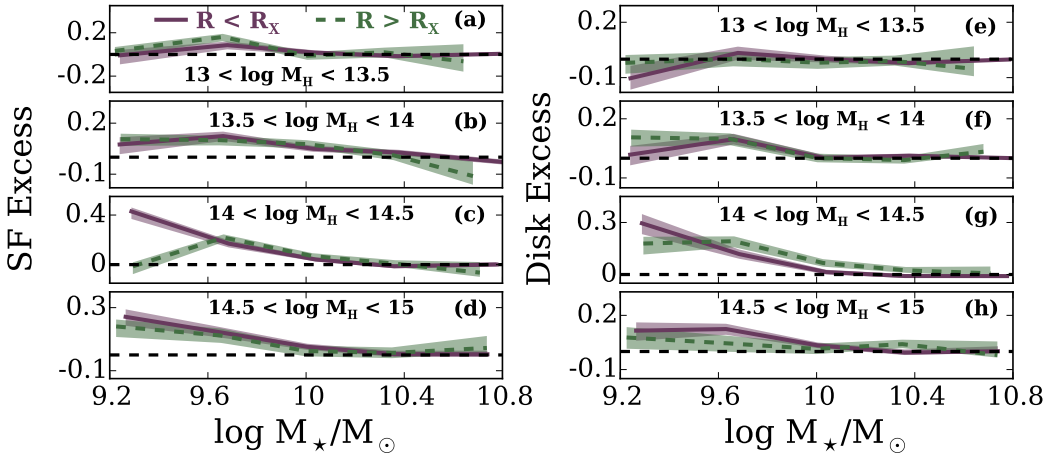

Figure 3.7 SF and disc excess versus stellar mass for both galaxies within (purple, solid) and outside (green, dashed) of the X-ray radius. Panels a-d show SF excess for four halo mass bins and panels e-h show disc excess for four halo mass bins. Shaded regions represent 1σ confidence intervals.

the X-ray radius, $R_{\rm Xray}$, given in Wang et al. 2014) and those galaxies that lie outside of the X-ray radius. We again plot star-forming/disc fraction versus stellar mass, in narrow halo mass bins, for the large and small radius subsamples. The results of this analysis are shown in Figs 3.5 and 3.6, where the two figures correspond to disc fraction and star-forming fraction trends for the large and small radius subsamples, respectively.

Examination of Figs 3.5 and 3.6 shows that for both galaxies found within their host halo's X-ray radius and those found outside, we still see an increase in star-forming and disc fractions in the XRW sample – as before this effect is strongest in the intermediate-to high-mass haloes and at low stellar mass. Also the disc and star-forming fractions tend to be higher at large radii, which is consistent with the morphology-density relation.

To further investigate if the increase in star-forming and disc fractions in the XRW sample compared to the XRS sample – which we will refer to as the 'SF excess' and the 'disc excess' – depends on whether you consider galaxies within or outside of the X-ray radius, we show SF and disc excess versus stellar mass in Fig. 3.7. We quantitatively define SF and disc excess as

$$\text{SF excess} = f_{SF}(\text{XRW}) - f_{SF}(\text{XRS}) \tag{3.6}$$

$$\text{Disc excess} = f_{D}(\text{XRW}) - f_{D}(\text{XRS}) \tag{3.7}$$

where f_{SF}(XRW) and f_{SF}(XRS) are the star-forming fractions in the XRW and XRS samples respectively, and analogously for f_D(XRW) and f_D(XRS).

We find no radial dependence for SF and disc excess as the two radial subsamples in Fig. 3.7 show overlap for all halo and stellar masses. With the exception in Fig. 3.7(c) where the SF excess, for low-mass galaxies, is stronger for galaxies within the X-ray radius.

3.4 Discussion

We find that star-forming and disc fractions are systematically lower in the XRS sample than galaxies in XRW environments. This trend persists even upon controlling for any halo mass dependence, however the observed difference between the XRS and the XRW sample is not enhanced when considering only those galaxies within the X-ray radius of the host halo.

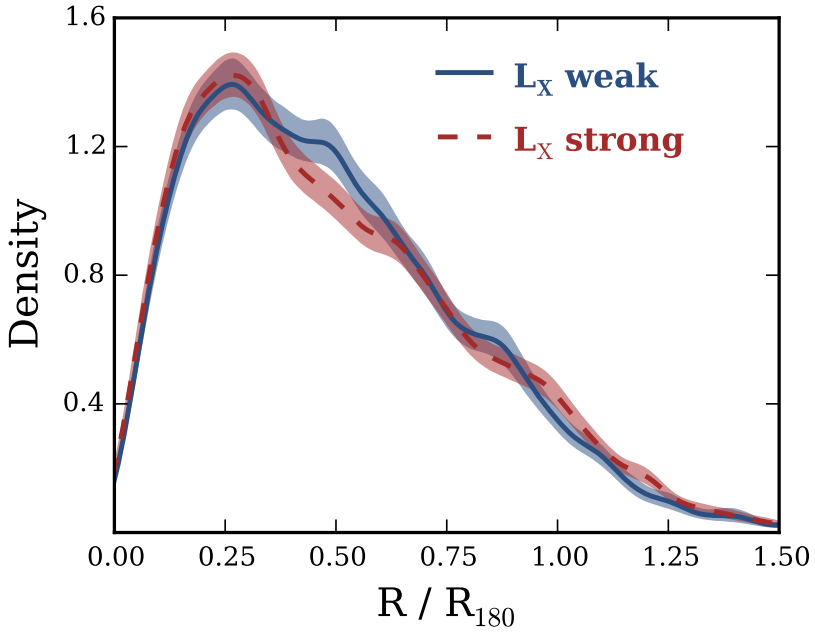

Figure 3.8 Smoothed radial distributions of galaxies in the XRW (blue, solid) and XRS (red, dashed) samples. Shaded regions correspond to 2σ confidence intervals obtained from random bootstrap resampling.

There are two major observed effects which have been found to impact the distributions of early-type and late-type galaxies within cluster environments. The so called 'Butcher-Oemler' (BO) effect is the observational trend that the blue fraction of cluster galaxies are positively correlated with redshift (e.g. Butcher & Oemler, 1984; Ellingson et al., 2001; Loh et al., 2008; Urquhart et al., 2010). However, it should be noted that there is still debate when it comes to the physical nature of the BO effect (for example, see: Andreon & Ettori 1999; Andreon et al. 2004, 2006. Since we are only considering low-redshift ($z < 0.1$) galaxies the BO effect should be negligible.

The second major effect is the previously mentioned morphology-density relationship. In order to determine if the morphology-density relation is affecting the trends we observe, we must check if there are significant differences in the radial distributions of the XRS and the XRW samples. For instance, if the XRW sample is found at systematically high group-centric radii compared to the XRS sample, then the morphology-density relation could explain why we find systematically larger star-forming and disc fractions in the XRW sample. In Fig. 3.8 we plot the smoothed radial distributions for both the XRS and the XRW samples. We see no systematic difference between the two distributions, in fact they are nearly indistinguishable from one another, and therefore any observed differences betwee the XRS and XRW samples are not being driven by differing radial distributions.

3.4.1 AGN contamination

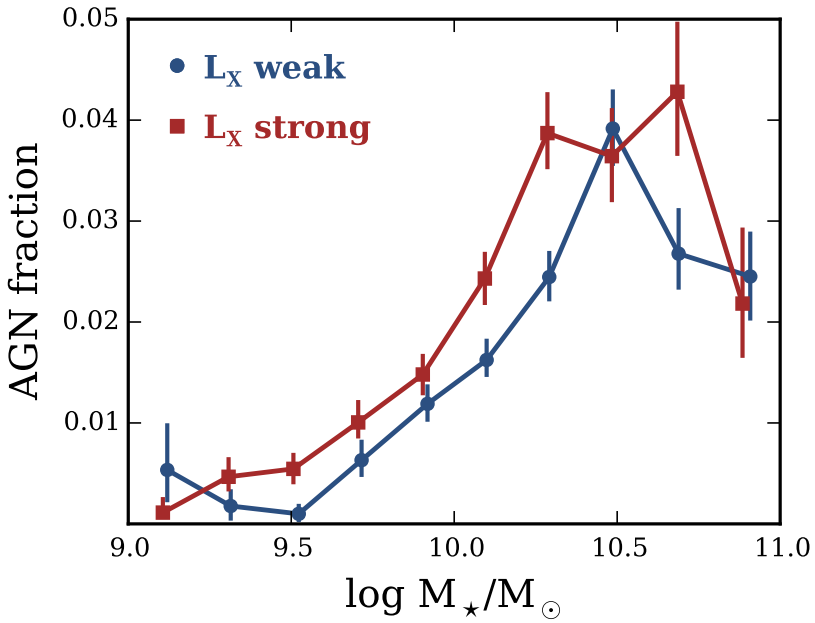

Figure 3.9 BPT identified AGN fraction versus stellar mass for the XRW and XRS samples. Error bars correspond to 1σ Bayesian binomial confidence intervals given in Cameron (2011).

When considering X-ray properties of galaxy groups it is important to ensure that the observed X-ray emission is due to the hot IGM and not due to contamination from AGN or other X-ray sources. In Wang et al. (2014) bright point sources, such as stars and quasars, are masked out, however it is still important to ensure that our results are not being contaminated by galaxies housing non-point source AGN.

In Fig. 3.9 we plot AGN fraction versus stellar mass for the XRW and XRS samples. We use AGN classified by Kauffmann et al. (2003), which are identified using the location of galaxies on the BPT diagram (Baldwin et al., 1981). I should be noted that Trouille & Barger (2010) show that between 20 and 50 per cent (depending on the dividing line between AGN and star-forming galaxies used) of X-ray identified AGN fail to be classified as AGN on the BPT diagram.

We see that the AGN fraction tends to be larger within the XRS sample, however at all stellar masses the number of AGN galaxies is a modest fraction (less than 5 per cent) of the total sample, for both XRS and XRW galaxies. Most relevant is the fact that at low stellar mass the AGN fraction is consistently below one per cent, for both the XRW and XRS samples, whereas the trends we observe with X-ray luminosity are exclusively seen at low stellar mass (e.g. Fig. 3.4). We examined disc and star-forming fractions for a subsample of the data with galaxies identified as AGN removed and found that removing AGN galaxies from the sample does not change the observed trends. Furthermore, we examined trends after removing all groups that house galaxies identified as AGN and again found no change in the observed trends. There-

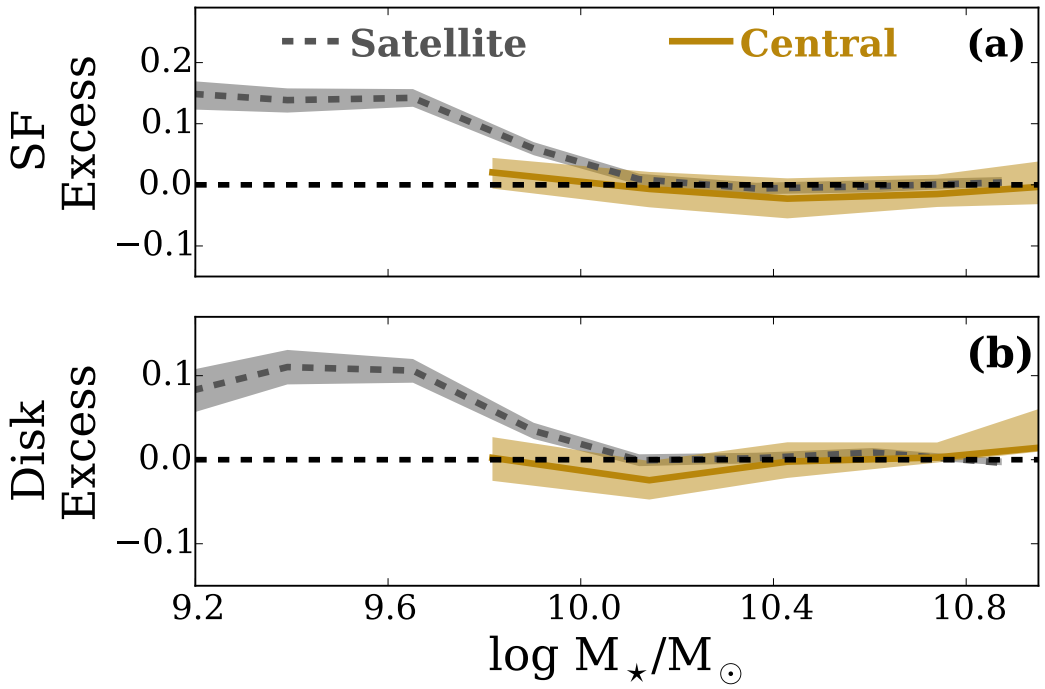

Figure 3.10 SF and disc excess versus stellar mass for both centrals (gold, solid) and satellites (grey, dashed). Shaded regions correspond to 1σ confidence intervals.

fore we conclude that AGN are not a significant contributor to the observed trends in star-forming and disc fractions.

3.4.2 Implications for star formation quenching

Tje relative importance of various galaxy quenching mechanisms is an important, open question. Galaxy populations in groups can be classified as either 'central' (located at the centre of the group dark matter halo) or 'satellite' galaxies. These two populations are expected to evolve differently (e.g. van den Bosch et al., 2008), and therefore when attempting to elucidate information on the quenching of galaxies it is important to consider centrals and satellites as

distinct populations. In Fig. 3.10 we plot SF and disc excess (equations 3.6 and 3.7) versus stellar mass, considering separately central and satellite galaxies. Central galaxies are defined as the most massive group galaxies and satellite galaxies are defined as all galaxies which have not been classified as centrals.

When considering satellite galaxies in Fig. 3.10(a) we find that galaxies within the XRW sample have consistently larger star-forming fractoins at low stellar mass (SF excess > 0), while at large stellar mass the XRW and XRS samples are indistinguishable. When considering only central galaxies we find that there is no difference between the XRW and XRS samples (SF excess ≈ 0) when considering star-forming fraction. We observe qualitatively similar trends for disc excess in Fig. 3.10(b). This implies that whatever effect X-ray luminosity has on star-forming and morphological properties it only affects satellite galaxies, central galaxies are insensitive to the group X-ray properties. This is not surprising given that central galaxies are massive, and we see no difference between the XRS and XRW at large stellar mass.

One interpretation of the differences we observe between the XRW and XRS samples would be to invoke the ram-pressure stripping of satellite galaxies. The rate at which galaxies will lose gas through ram-pressure stripping will increase in proportion to L_X (Fairley et al., 2002). Therefore if ram-pressure is an important mechanism when it comes to the quenching of galaxies, a decrease in star-forming fraction should be observed with increasing X-ray luminosity. It should be noted that although we observe very similar trends for star-forming and disc fractions, it is not clear whether ram-pressure stripping can efficiently drive galaxy morphology transformations from late to early

type (Christlein & Zabludoff, 2004). Prior studies (e.g. Gavazzi et al., 2003; Kenney et al., 2004; Muzzin et al., 2014) have found evidence of ram-pressure stripping. We note as well that other studies (e.g. Balogh et al., 2002a; Fairley et al., 2002; Wake et al., 2005; Lopes et al., 2014) have found no clear trend between star-forming or blue fractions and X-ray luminosity. At first glance the results shown in Fig. 3.4 are consistent with ram-pressure stripping; at low stellar masses there are lower star-forming fractions in the XRS sample. One difference between the results we observe and previous studies is that we narrowly bin our data in stellar mass. Since star-forming and morphological properties depend strongly on stellar mass, any residual dependence on X-ray luminosity may be lost without controlling for stellar mass. In addition our sample size is significantly larger than most previous studies, so it may be that trends with X-ray luminosity are subtle enough to be missed without large statistics.

If the trends we detect are driven by ram-pressure we would expect a radial dependence of our trends with X-ray luminosity. The efficiency of ram-pressure stripping is proportional to ρv^2 (Wake et al., 2005; Popesso et al., 2007b), where ρ is the IGM density and v is the speed of the member galaxies. Since the IGM density is highest at small group-centric radii, the efficiency of ram-pressure stripping should increase towards small radii. In Fig. 3.7 we showed that the observed SF excess does not strongly depend on radius. We conclude that this lack of radial dependence is inconsistent with the ram-pressure stripping scenario.

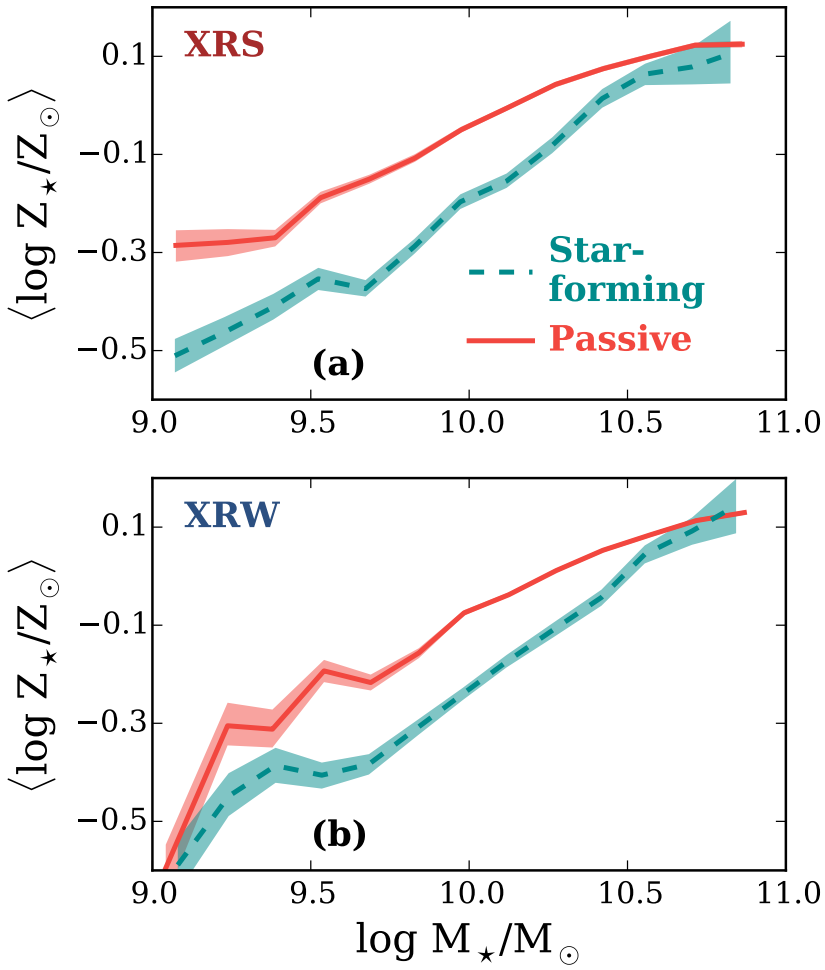

Figure 3.11 Mean stellar metallicity versus stellar mass for star-forming (blue, dashed) and passive (red, solid) galaxies, divided by galaxies in the XRS (top) and XRW (bottom) samples. Shaded regions correspond to 1σ confidence intervals obtained from random bootstrap resampling.

Another often-envoked mechanism for regulating star formation is 'galaxy strangulation' (Larson et al., 1980; Balogh et al., 2000; Kawata & Mulchaey, 2008; Peng et al., 2015). Strangulation is a mechanism in which the replenishment of cold gas on to galaxies is halted, which in turn leads to galaxy quenching once the galaxy has exhausted its existing cold gas reservoirs. The time-scales over which a galaxy will be quenched by strangulation are longer than the times associated with the direct stripping of cold gas reserves (ram-pressure). Recently, Peng et al. (2015) have argued that it is possible to differentiate between strangulation and direct stripping using metallicity differences between star-forming and quiescent galaxy populations. We direct the reader to Peng et al. (2015) for a more complete discussion, however the main idea is that quenching by strangulation will result in higher metallicities for passive galaxies compared to star-forming galaxies. This is a result of star formation continuing even after the gas supply has been halted which will increase stellar metallicity until the cold gas reserves have been exhausted and the galaxy has therefore been quenched. This trend in metallicity is not expected from direct stripping, where star formation shuts off quickly after the removal of cold gas.

To investigate the effect of strangulation on the galaxy sample in this study we follow Peng et al. (2015) and calculate mean stellar metallicity versus stellar mass considering star-forming and passive galaxies separately, for galaxies within our XRW sample as wel as our XRS sample. Metallicities are matched to our sample from the catalogue of Gallazzi et al. (2005), and mean metallicities are calculated in stellar mass bins with widths of 0.15 dex. Not all of the galaxies within this sample have measured metallicities, and our XRW and

XRS samples are reduced to 10 939 (52 per cent of total sample) and 8 851 (44 per cent of total sample) member galaxies respectively.

In Fig. 3.11 we see higher stellar metallicities for passive galaxies compared to star-formers, which we interpret as evidence for strangulation playing a significant role in star formation quenching. Of particular interest for this work is the behaviour at low stellar mass which is where the dependence of star formation and morphology on X-ray luminosity is observed (see Fig. 3.4). We see a somewhat stronger strangulation signal (ie. difference between passive and star-former metallicity) for galaxies in the XRS sample compared to the XRW sample, at low stellar mass.

In light of this observed difference, it is important to note that compiling this subsample of galaxies with measured metallicities does not affect all stellar masses equally. Specifically, low-mass galaxies are preferentially removed from the sample when matching to the metallicity catalogue. In particular, 69 per cent of low-mass ($M_\star < 10^{9.5}\mathrm{M}_\odot$) galaxies in the XRS sample do not have measured metallicities, whereas in the XRW sample 75 per cent of low-mass galaxies do not ahve measured metallicities. Not only are low-mass galaxies being preferentially lost, but the fraction of low-mass galaxies being lost is slightly different between the two X-ray samples. Therefore, although the results in Fig. 3.11 are consistent with strangulation – and more specifically, somewhat stronger strangulation at the low-mass end of the XRS sample – we suggest that this trend be interpreted with caution as completeness differences could be playing some role.

3.4.3 Group evolutionary/dynamical state

The dynamical state of galaxy groups is an important evolutionary indicator and can potentially influence galaxy properties. Trends with X-ray luminosity may reflect that the XRW and XRS samples have different dynamical properties as it is expected that more evolved groups with relaxed dynamics would be more X-ray luminous (Popesso et al., 2007a).

Theoretically the velocity distribution of galaxies within a group in dynamical equilibrium should have a characteristic Gaussian shape. Groups lacking this Gaussian distribution can therefore be considered as being unevolved, dynamically young systems. To investigate the dependence on the dynamical state of the groups in our data set we follow the procedure of Hou et al. (2009) and apply the Anderson-Darling normality (ADN) test to the velocity distributions of the galaxies in the group sample. The ADN test is a non-parametric test which compares the cumulative distribution function (CDF) of the data to the CDF of a normal distribution to determine the probability (p-value) that the difference between the distribution of the data and that of a Gaussian is as large as observed (or larger), under the assumption that the data is in fact normally distributed. For our dynamical analysis we use a subset of the data consisting of only those groups with eight or more members (31 820 galaxies in 1 456 groups), in order to ensure reasonable statistics when applying the ADN test. To obtain values for the ADN statistic for each of our groups we employ the `ad.test {nortest}` function in the statistical computing language R (R Core Team, 2013) – large values of the ADN statistic are indicative of less Gaussian distributions.

Initially, we examine the dynamical states of galaxies within the XRW and XRS samples globally (ie. no radial cuts) and we find no systematic differences between the dynamical states of XRW and XRS galaxies. Popesso et al. (2007a) study the difference between X-ray underluminous Abell (AXU) clusters and normal Abell clusters. They find that while both AXU and normal Abell clusters show Gaussian velocity distributions within the virialized region ($R < 1.5\,\mathrm{R}_{200}$), within the exterior regions ($1.5 \leq R \leq 3.5\,\mathrm{r}_{200}$) the AXU cluster show sharply peaked, non-Gaussian velocity distributions. The authors interpret these leptokurtic velocity distributions in the outer cluster regions as evidence that AXU clusters have experienced recent accretion/merging. If the XRW groups have experienced more recent accretion of galaxies from the field and smaller groups than the XRS groups, then this could contribute to the dependence we observe between star-forming and disc fractions on X-ray luminosity. Galaxies in underdense regions (the field, low-mass groups) have been found to be preferentially star- forming with late-type morphologies. Accordingly, groups experiencing recent accretion may contain more star-forming, late-type, galaxies when compared to groups which are dynamically older.

To investigate this possibility we study the dynamical states of groups in both the XRW and XRS samples, and divide member galaxies into two radial subsamples: those found in the inner regions ($R < R_{180}$) of their host group, and those found in the outer regions ($R \geq R_{180}$) of their host group. This is similar to the analysis performed by Popesso et al. (2007a). Instead of making an arbitrary, discrete cut to define Gaussian and non-Gaussian groups we treat the AD statistic values as continuous and compare the distributions of ADN statistics from the four subsamples (XRW inner, XRW outer, XRS

inner, XRS outer) to determine whether there are any significant differences in dynamical state. To quantitatively compare the distributions we utilize the two-sample Anderson-Darling (AD2) test. The AD2 test is similar to the ADN test, however instead of comparing observed data to the normal distribution, it compares the CDFs of two data samples to determine whether they are drawn from the same underlying distribution. We apply the AD2 test to the distributions of ADN statistic values for the XRW and XRS samples to determine if the dynamical states vary between the inner and the outer regions. To perform the AD2 test between the subsamples we use the `ad.test {kSamples}` function in the statistical computing language R (R Core Team, 2013).

We find no evidence ($\mathrm{p-value} = 0.38$) for different dynamical states in the inner and outer regions of the XRS sample, however for the XRW sample we find strong evidence ($\mathrm{p-value} = 3 \times 10^{-7}$) that the dynamical state of galaxies in the outer region is different from those in the inner region. When we examine the distributions of ADN statistics for the four subsamples we find that the ADN statistic values for the XRW outer subsample are systematically higher than for the other three subsamples. This suggests that the velocity distributions for galaxies outside of the virial radius in the XRW sample are less Gaussian than the rest of the data set.

This result is consistent with Popesso et al. (2007a), who find non-Gaussian velocity distributions for galaxies in the outer regions of X-ray underluminous Abell clusters. This result supports the notion that the increased number of star-forming and late-type galaxies we observe in the XRW sample can potentially be explained by underluminous X-ray groups experiencing recent accre-

tion of field galaxies and small galaxy groups, as this recent accretion can give rise to less Gaussian velocity distributions in the exteriors of these groups.

We do note that it remains difficult to simultaneously explain the dynamical results together with the fact that we observe no dependence of SF and disc excess on radius (Fig. 3.7).

3.5 Summary & Conclusions

We have used a sample of galaxies taken from X-ray emitting groups and clusters in the SDSS to study the effect of X-ray luminosity on galaxy star formation and morphological properties. Using a data set spanning a large range in stellar mass ($10^{9} - 10^{11.3}\mathrm{M}_{\odot}$), halo mass ($10^{13} - 10^{15}\mathrm{M}_{\odot}$), and X-ray luminosity ($10^{39.6} - 10^{46.4}\mathrm{erg\,s^{-1}}$) we have investigated the differences between disc and star-forming fractions within different X-ray environments. The main results of this paper are as follows.

(i) Star-forming and disc fractions are preferentially lower within the X-ray strong sample when compared to galaxies within the X-ray weak sample – this trend remains after controlling for any halo mass dependence.

(ii) This difference between the X-ray strong and X-ray weak samples is most apparent at intermediate to high halo mass and at low stellar mass.

(iii) The differences we observe between the X-ray weak and X-ray strong samples do not depend on whether we consider galaxies inside of, or outside their host halo's X-ray radius.

(iv) The enhancement of star-forming and disc fractions we observe in the X-ray weak sample is present for satellites but not central galaxies, which is not surprising given that the difference between X-ray samples is only seen at low stellar mass.

(v) Our results are consistent with quenching by strangulation, in particular we see a somewhat stronger strangulation signal at low stellar mass within the XRS sample.

Bibliography

Abazajian, K. N., Adelman-McCarthy, J. K., Agüeros, M. A., Allam, S. S., Allende Prieto, C., An, D., Anderson, K. S. J., Anderson, S. F., Annis, J., Bahcall, N. A., & et al. 2009, ApJS, 182, 543

Andreon, S. & Ettori, S. 1999, ApJ, 516, 647

Andreon, S., Lobo, C., & Iovino, A. 2004, MNRAS, 349, 889

Andreon, S., Quintana, H., Tajer, M., Galaz, G., & Surdej, J. 2006, MNRAS, 365, 915

Baldwin, J. A., Phillips, M. M., & Terlevich, R. 1981, PASP, 93, 5

Balogh, M., Bower, R. G., Smail, I., Ziegler, B. L., Davies, R. L., Gaztelu, A., & Fritz, A. 2002a, MNRAS, 337, 256

Balogh, M. L., Baldry, I. K., Nichol, R., Miller, C., Bower, R., & Glazebrook, K. 2004, ApJ, 615, L101

Balogh, M. L., Navarro, J. F., & Morris, S. L. 2000, ApJ, 540, 113

Balogh, M. L., Smail, I., Bower, R. G., Ziegler, B. L., Smith, G. P., Davies, R. L., Gaztelu, A., Kneib, J.-P., & Ebeling, H. 2002b, ApJ, 566, 123

Barnes, J. 1985, MNRAS, 215, 517

Blanton, M. R., Eisenstein, D., Hogg, D. W., Schlegel, D. J., & Brinkmann, J. 2005a, ApJ, 629, 143

Blanton, M. R. & Roweis, S. 2007, AJ, 133, 734

Blanton, M. R., Schlegel, D. J., Strauss, M. A., Brinkmann, J., Finkbeiner, D., Fukugita, M., Gunn, J. E., Hogg, D. W., Ivezić, Ž., Knapp, G. R., Lupton, R. H., Munn, J. A., Schneider, D. P., Tegmark, M., & Zehavi, I. 2005b, AJ, 129, 2562

Brinchmann, J., Charlot, S., White, S. D. M., Tremonti, C., Kauffmann, G., Heckman, T., & Brinkmann, J. 2004, MNRAS, 351, 1151

Brough, S., Forbes, D. A., Kilborn, V. A., & Couch, W. 2006, MNRAS, 370, 1223

Butcher, H. & Oemler, Jr., A. 1978, ApJ, 219, 18

—. 1984, ApJ, 285, 426

Cameron, E. 2011, PASA, 28, 128

Christlein, D. & Zabludoff, A. I. 2004, ApJ, 616, 192

Chung, A., van Gorkom, J. H., Kenney, J. D. P., & Vollmer, B. 2007, ApJ, 659, L115

De Lucia, G., Weinmann, S., Poggianti, B. M., Aragón-Salamanca, A., & Zaritsky, D. 2012, MNRAS, 423, 1277

Dressler, A. 1980, ApJ, 236, 351

Dressler, A., Smail, I., Poggianti, B. M., Butcher, H., Couch, W. J., Ellis, R. S., & Oemler, Jr., A. 1999, ApJS, 122, 51

Ellingson, E., Lin, H., Yee, H. K. C., & Carlberg, R. G. 2001, ApJ, 547, 609

Fairley, B. W., Jones, L. R., Wake, D. A., Collins, C. A., Burke, D. J., Nichol, R. C., & Romer, A. K. 2002, MNRAS, 330, 755

Gallazzi, A., Charlot, S., Brinchmann, J., White, S. D. M., & Tremonti, C. A. 2005, MNRAS, 362, 41

Gavazzi, G., Cortese, L., Boselli, A., Iglesias-Paramo, J., Vílchez, J. M., & Carrasco, L. 2003, ApJ, 597, 210

Gunn, J. E. & Gott, III, J. R. 1972, ApJ, 176, 1

Hou, A., Parker, L. C., Balogh, M. L., McGee, S. L., Wilman, D. J., Connelly, J. L., Harris, W. E., Mok, A., Mulchaey, J. S., Bower, R. G., & Finoguenov, A. 2013, MNRAS, 435, 1715

Hou, A., Parker, L. C., & Harris, W. E. 2014, MNRAS, 442, 406

Hou, A., Parker, L. C., Harris, W. E., & Wilman, D. J. 2009, ApJ, 702, 1199

Hoyle, B., Masters, K. L., Nichol, R. C., Jimenez, R., & Bamford, S. P. 2012, MNRAS, 423, 3478

Huchra, J. P. & Geller, M. J. 1982, ApJ, 257, 423

Kauffmann, G., Heckman, T. M., Tremonti, C., Brinchmann, J., Charlot, S., White, S. D. M., Ridgway, S. E., Brinkmann, J., Fukugita, M., Hall, P. B., Ivezić, Ž., Richards, G. T., & Schneider, D. P. 2003, MNRAS, 346, 1055

Kawata, D. & Mulchaey, J. S. 2008, ApJ, 672, L103

Kenney, J. D. P., van Gorkom, J. H., & Vollmer, B. 2004, AJ, 127, 3361

Lackner, C. N. & Gunn, J. E. 2013, MNRAS, 428, 2141

Larson, R. B., Tinsley, B. M., & Caldwell, C. N. 1980, ApJ, 237, 692

Loh, Y.-S., Ellingson, E., Yee, H. K. C., Gilbank, D. G., Gladders, M. D., & Barrientos, L. F. 2008, ApJ, 680, 214

Lopes, P. A. A., Ribeiro, A. L. B., & Rembold, S. B. 2014, MNRAS, 437, 2430

Mantz, A., Allen, S. W., Ebeling, H., Rapetti, D., & Drlica-Wagner, A. 2010, MNRAS, 406, 1773

McGee, S. L., Balogh, M. L., Bower, R. G., Font, A. S., & McCarthy, I. G. 2009, MNRAS, 400, 937

Moore, B., Katz, N., Lake, G., Dressler, A., & Oemler, A. 1996, Nature, 379, 613

Muzzin, A., van der Burg, R. F. J., McGee, S. L., Balogh, M., Franx, M., Hoekstra, H., Hudson, M. J., Noble, A., Taranu, D. S., Webb, T., Wilson, G., & Yee, H. K. C. 2014, ApJ, 796, 65

Muzzin, A., Wilson, G., Yee, H. K. C., Gilbank, D., Hoekstra, H., Demarco, R., Balogh, M., van Dokkum, P., Franx, M., Ellingson, E., Hicks, A., Nantais, J., Noble, A., Lacy, M., Lidman, C., Rettura, A., Surace, J., & Webb, T. 2012, ApJ, 746, 188

Navarro, J. F., Frenk, C. S., & White, S. D. M. 1997, ApJ, 490, 493

Peng, Y., Maiolino, R., & Cochrane, R. 2015, Nature, 521, 192

Peng, Y.-j., Lilly, S. J., Kovač, K., Bolzonella, M., Pozzetti, L., Renzini, A., Zamorani, G., Ilbert, O., Knobel, C., Iovino, A., Maier, C., Cucciati, O., Tasca, L., Carollo, C. M., Silverman, J., Kampczyk, P., de Ravel, L., Sanders, D., Scoville, N., Contini, T., Mainieri, V., Scodeggio, M., Kneib, J.-P., Le Fèvre, O., Bardelli, S., Bongiorno, A., Caputi, K., Coppa, G., de la Torre, S., Franzetti, P., Garilli, B., Lamareille, F., Le Borgne, J.-F., Le Brun, V., Mignoli, M., Perez Montero, E., Pello, R., Ricciardelli, E., Tanaka, M., Tresse, L., Vergani, D., Welikala, N., Zucca, E., Oesch, P., Abbas, U., Barnes, L., Bordoloi, R., Bottini, D., Cappi, A., Cassata, P., Cimatti, A., Fumana, M., Hasinger, G., Koekemoer, A., Leauthaud, A., Maccagni, D., Marinoni, C., McCracken, H., Memeo, P., Meneux, B., Nair, P., Porciani, C., Presotto, V., & Scaramella, R. 2010, ApJ, 721, 193

Popesso, P., Biviano, A., Böhringer, H., & Romaniello, M. 2007a, A&A, 461, 397

Popesso, P., Biviano, A., Romaniello, M., & Böhringer, H. 2007b, A&A, 461, 411

Postman, M., Franx, M., Cross, N. J. G., Holden, B., Ford, H. C., Illingworth, G. D., Goto, T., Demarco, R., Rosati, P., Blakeslee, J. P., Tran, K.-V., Benítez, N., Clampin, M., Hartig, G. F., Homeier, N., Ardila, D. R., Bartko, F., Bouwens, R. J., Bradley, L. D., Broadhurst, T. J., Brown, R. A., Burrows, C. J., Cheng, E. S., Feldman, P. D., Golimowski, D. A., Gronwall, C., Infante, L., Kimble, R. A., Krist, J. E., Lesser, M. P., Martel, A. R., Mei, S., Menanteau, F., Meurer, G. R., Miley, G. K., Motta, V., Sirianni,

M., Sparks, W. B., Tran, H. D., Tsvetanov, Z. I., White, R. L., & Zheng, W. 2005, ApJ, 623, 721

Postman, M. & Geller, M. J. 1984, ApJ, 281, 95

R Core Team. 2013, R: A Language and Environment for Statistical Computing, R Foundation for Statistical Computing, Vienna, Austria

Shen, S., Kauffmann, G., von der Linden, A., White, S. D. M., & Best, P. N. 2008, MNRAS, 389, 1074

Simard, L., Mendel, J. T., Patton, D. R., Ellison, S. L., & McConnachie, A. W. 2011, ApJS, 196, 11

Trouille, L. & Barger, A. J. 2010, ApJ, 722, 212

Urquhart, S. A., Willis, J. P., Hoekstra, H., & Pierre, M. 2010, MNRAS, 406, 368

van den Bosch, F. C., Aquino, D., Yang, X., Mo, H. J., Pasquali, A., McIntosh, D. H., Weinmann, S. M., & Kang, X. 2008, MNRAS, 387, 79

Wake, D. A., Collins, C. A., Nichol, R. C., Jones, L. R., & Burke, D. J. 2005, ApJ, 627, 186

Wang, L., Yang, X., Shen, S., Mo, H. J., van den Bosch, F. C., Luo, W., Wang, Y., Lau, E. T., Wang, Q. D., Kang, X., & Li, R. 2014, MNRAS, 439, 611

Wetzel, A. R., Tinker, J. L., & Conroy, C. 2012, MNRAS, 424, 232

Whitaker, K. E., van Dokkum, P. G., Brammer, G., & Franx, M. 2012, ApJ, 754, L29

Yang, X., Mo, H. J., van den Bosch, F. C., & Jing, Y. P. 2005, MNRAS, 356, 1293

Yang, X., Mo, H. J., van den Bosch, F. C., Pasquali, A., Li, C., & Barden, M. 2007, ApJ, 671, 153

This page intentionally left blank.